INSTITUTO DE HIGIENE E
MEDICINA TROPICAL
DESDE 1902

UNIVERSIDADE
NOVA
DE LISBOA

Universidade Nova de Lisboa

Instituto de Higiene e Medicina Tropical

ANTIBACTERIAL, ANTIPARASITIC AND ANTICANCER PROPERTIES OF HOST-DEFENCE PEPTIDES FROM ARGENTINIAN AMPHIBIANS

Miriam Raquel Figueiredo Arrulo

THESIS SUBMITTED TO OBTAIN A MASTER'S DEGREE IN BIOMEDICAL SCIENCES

OCTOBER, 2019

Universidade Nova de Lisboa

Instituto de Higiene e Medicina Tropical

ANTIBACTERIAL, ANTIPARASITIC AND ANTICANCER PROPERTIES OF HOST-DEFENCE PEPTIDES FROM ARGENTINIAN AMPHIBIANS

Author: Miriam Raquel Figueiredo Arrulo

Supervisor: Dr Peter Eaton

Co-Supervisor: Dr Celso Cunha

Thesis submitted to obtain a Master's Degree in Biomedical Sciences

Project developed at:

Bibliographic elements resulting from this thesis

Posters:

Miriam F. Arrulo, Constança P. Amaral, Mariela M. Marani, Natalia Lorena Cancelarich, Marco M. Domingues, Margarida Sanches-Vaz, Luísa M. Figueiredo, Nuno C. Santos, Peter Eaton. July 2019. Anticancer and Antimicrobial Properties of Host-defence Peptides from Patagonian Amphibians. 4th Meeting of the College of Chemistry (4ECQUL). Lisbon, Portugal.

Dedication

In memory of my grandma Ricardina whose unyielding strength and love made me who I am today.

"Chaos is merely order waiting to be deciphered."

José Saramago

Acknowledgements

I would like to thank my family, especially mum, dad and my brother for their unconditional love and support. Without you this endeavour would have never been possible.

To Jon, my brave fiancé, who left his life in England to go on this adventure with me and who has been a tireless listener to all my worries and victories for the past two years.

To the two gems in my life, Paddy and Tommy, for making me smile every time with your wagging tails and endless cuddles.

A special thank you to my colleagues and lecturers at the *"Instituto de Higiene e Medicina Tropical – Universidade NOVA de Lisboa"* for all their support, advice and encouragement. You inspired me to work harder and believe that nothing is impossible once you set your mind to it.

I would also like to express my gratitude to our Argentinian partners from IPEEC-CONICET, Dr Mariela M. Marani and PhD student Natalia Lorena Cancelarich, for providing the peptides used in this study. Also, a thank you to Diana Fontinha, PhD, from Miguel Prudêncio Lab (iMM) for supplying the cells used in the anticancer assays, and to the Luísa Figueiredo Lab and Margarida Sanches-Vaz (iMM) for donating the trypanosomes and offering the necessary facilities that allowed for antiparasitic testing.

Last but not least, a big thank you to the "*Instituto de Medicina Molecular João Lobo Antunes*", the whole team (and yes I really mean everybody!) at Nuno Santos Lab (iMM) and to Dr Peter Eaton and Constança Amaral for accepting me for this project and teaching me so much more than what I could have anticipated. You guys were fab and I shall miss you all very much.

Declaration of authorship

I, Miriam Raquel Figueiredo Arrulo, declare that this thesis and the work presented in it are my own and have been generated by me as the result of my own original research.

I confirm that:

1. Where I have consulted the published work of others, this is always clearly attributed;

4. Where I have quoted from the work of others, the source is always given. With the exception of such quotations, this thesis is entirely my own work;

5. I have recognized all main sources of help.

For the information and results present in this thesis that have been supplied by partner labs and/or collaborators, I acknowledge and confirm that:

a) The work performed on peptide identification, sequencing and antimicrobial testing (except for the antimicrobial activity of peptide Ooc-1) is part of Lorena Cancelarich's PhD thesis (not yet published) from Mariela M. Marani's Lab at the "*Instituto Patagónico para el Estudio de los Ecosistemas Continentales*" (IPEEC-CONICET) in Argentina and this is made clear throughout the thesis;

b) The apoptosis/necrosis assay authorship rests solely with PhD student Constança P. Amaral, from Nuno Santos Lab at the "*Instituto de Medicina Molecular João Lobo Antunes*" in Lisbon, was carried out in Brazil and this is also acknowledged appropriately in the thesis.

c) Either none of this work has been published before submission, or parts of this work have been published as:

Marani MM, Perez LO, de Araujo AR, Plácido A, Sousa CF, Quelemes PV, et al. Thaulin-1: The first antimicrobial peptide isolated from the skin of a Patagonian frog *Pleurodema thaul* (Anura: Leptodactylidae: Leiuperinae) with activity against *Escherichia coli*. Gene [Internet] 2017;605(March):70–80.
doi: 10.1016/j.gene.2016.12.020

Resumo

Os péptidos de defesa do hospedeiro (PDH) são geralmente moléculas curtas, anfipáticas e catiónicas que fazem parte do sistema imune inato da maioria dos organismos multicelulares. Inicialmente descritos como péptidos antimicrobianos (PAMs) devido à interação e destruição de paredes celulares bacterianas que são naturalmente aniónicas, contudo, estudos recentes mostraram que os PDH possuem uma gama de ação mais variada sendo capazes de interagir com células cancerígenas e podendo assim também ser designados de péptidos anticancerígenos (PACs).

O aumento da multirresistência a fármacos, juntamente com a baixa taxa de descoberta de novos compostos e o facto de os tratamentos atualmente utilizados na terapêutica de várias doenças poderem ser abrasivos e até prejudiciais aos seres humanos, culminaram na necessidade urgente de estudar novas alternativas como os PDH.

Várias espécies de anfíbios Patagónicos adaptaram-se a sobreviver em condições climáticas adversas, habitando zonas áridas ou semiáridas da Patagónia. A pele destes anfíbios produz uma secreção protetora a partir da qual os PDH foram extraídos, identificados e sintetizados nos péptidos PSo-4, PSo-7, PSo2-2, Thau-3 e Ooc-1.

O objetivo deste trabalho foi caracterizar as propriedades antimicrobianas e anticancerígenas dos referidos péptidos e a sua estrutura em solução e na presença de vesículas lipídicas.

A atividade antimicrobiana bem como a interação com membranas bacterianas foram avaliadas em bactérias Gram-positivas e -negativas por determinação da concentração mínima inibitória e através de microscopia de força atómica. Foram ainda realizados ensaios antiparasitários em formas sanguíneas, tipo selvagem, de *Trypanosoma brucei brucei*, ao passo que estudos anticancerígenos foram praticados em células Huh-7 de carcinoma hepatocelular humano através de métodos fluorimétricos e de absorção respetivamente. A caracterização da conformação dos péptidos, quando em meio aquoso ou em solução contendo vesículas lipídicas POPC:POPG, foi realizada por ensaios de espectrofluorometria e de dicroísmo circular.

PSo-4, PSo-7, Thau-3 e Ooc-1 exibiram atividade antimicrobiana, mas apenas contra *E. coli*. PSo-4 demonstrou a atividade mais forte enquanto Ooc-1 provou ser bactericida. A análise por AFM apoia a hipótese de que a ação destes péptidos possa ocorrer ao nível da parede celular bacteriana, ou potencialmente interferindo com vias ou alvos intracelulares, culminando na desintegração da célula. Resultados preliminares também indicam que o péptido Ooc-1 exerce efeitos inibitórios no parasita *T. b. brucei*. Além disso, os péptidos Pso-7, Pso-4 e PSo2-2 revelaram potencial nocivo contra células Huh-7. Estruturalmente, a maioria dos péptidos apresentou propensão à agregação, quando em solução, e estrutura secundária com algum conteúdo de α-hélice, contrariamente a PSo-7 e PSo-4 que mantiveram uma disposição aleatória e baixos níveis de agregação.

Tendo em consideração o comportamento e raio de ação demonstrados, é nossa convicção de que estes péptidos seriam dignos candidatos a investigação adicional e possível manipulação a nível da sua sequência, com o fim de aperfeiçoar as capacidades demonstradas de modo a abrir um caminho viável de desenvolvimento farmacológico.

Palavras-chave: Péptidos anticancerígenos, péptidos antimicrobianos, péptidos antiparasitários, péptidos de defesa do hospedeiro, péptidos de anfíbios Patagónicos.

Abstract

Host-defence peptides (HDPs) are usually short, cationic and amphipathic molecules that are part of the innate immune system of most multicellular organisms. Initially described as antimicrobial peptides (AMPs) due to their interaction and destruction of bacterial cell walls which are naturally anionic, however, recent studies have shown that HDPs have a broader range of action being able to interact with cancer cells and may therefore also be referred to as anticancer peptides (ACPs).

Increasing worldwide multidrug resistance (MDR) together with the low discovery rate of new drugs and the fact that the current treatments used in the therapy of various diseases can be very harsh and damaging to human beings, culminated in an urgent need to study new alternatives such as HDPs.

Several species of Patagonian amphibians have adapted to survive in adverse climatic conditions, inhabiting arid or semi-arid zones of Patagonia. The skin of these amphibians produces a protective secretion from which the HDPs were extracted, identified and synthesized into peptides PSo-4, PSo-7, PSo2-2, Thau-3 and Ooc-1.

The aim of this work was to characterize the antimicrobial and anticancer properties of the peptides mentioned as well as their structure in solution and in the presence of lipid vesicles.

Antimicrobial activity and interaction with bacterial membranes were assessed in Gram-positive and Gram-negative bacteria by minimal inhibitory concentration determination and atomic force microscopy. In addition, antiparasitic assays were carried out on wild-type bloodstream forms of *Trypanosoma brucei brucei* while anticancer studies were performed on human hepatocellular carcinoma Huh-7 cells through fluorescence and absorption spectrophotometry methods respectively. The characterization of the peptides conformation when in aqueous medium or in a solution containing POPC:POPG lipid vesicles was done via spectrofluorometric and circular dichroism assays

PSo-4, PSo-7, Thau-3 and Ooc-1 exhibited antimicrobial activity but only against the Gram-positive bacteria *E. coli*. PSo-4 showed the strongest activity while Ooc-1 proved to be bactericidal. Analysis by AFM supports the hypothesis that the action of these peptides may occur either at the bacterial cell wall level or by potentially interfering with intracellular pathways or targets, culminating in cell disintegration. Preliminary results also indicate that peptide Ooc-1 exerts inhibitory effects on the parasite *T. brucei brucei*. Furthermore, peptides PSo-7, PSo-4, and PSo2-2 revealed deleterious capacity against Huh-7 cells. Structurally most peptides exhibited a propensity for aggregation, when in solution, and presented a secondary structure with some α-helix content, except for PSo-7 and PSo-4 that maintained a random coil arrangement and lower aggregation levels.

Considering the behaviour and scope of action demonstrated, we believe these peptides to be worthy candidates for further investigation and possible sequence manipulation to enhance their demonstrated capabilities in order to open the path of pharmacological viability.

Keywords: Anticancer peptides, antimicrobial peptides, antiparasitic peptides, host-defence peptides, Patagonian amphibians' peptides.

Table of Contents

List of Figures

List of Tables

Symbols and Abbreviations

≈	Approximately equal
~	Approximately equal – weak approximation
°C	Degree centigrade
%	Percentage
3D	Three-dimensional
α	Alpha
A	Absorbance
β	Beta
λ	Wavelength
λ$_{Em}$	Wavelength emission
λ$_{Exc}$	Wavelength excitation
λ$_{max}$	Wavelength of fluorescence intensity maximum
θ	Degrees of ellipticity
ACP(s)	Anticancer peptide(s)
AFM	Atomic force microscopy
Ala (A)	Alanine
AMP(s)	Antimicrobial peptide(s)
ANOVA	Analysis of variance
ANS	8-anilino-1-naphthalenesulfonic acid
APD	Antimicrobial peptide database
Arg (R)	Arginine
Asn (N)	Asparagine
AT	African trypanosomiasis
A.U.	Arbitrary units
BBB	Blood-brain barrier
BSF(s)	Bloodstream form(s)

C	Carboxyl group
Ca^{2+}	Calcium ion
CD	Circular dichroism
cfu	Colony-forming unit(s)
CLSI	Clinical Laboratory Standards Institute
cm^2	Square centimetre
CNS	Central nervous system
CSF	Cerebrospinal fluid
Cys (C)	Cysteine
deg	Degree
dmol	Decimol
DNA	Deoxyribonucleic acid
E	Magnitude of electric field vector
F_I	Fluorescence emission intensity
F_{Imax}	Fluorescence emission intensity maximum
FTIR	Fourier-transform infrared spectroscopy
Gln (Q)	Glutamine
Gly (G)	Glycine
h	Hour
HMI	Hirumi modified Iscove
HAT	Human African trypanosomiasis
HCC	Human hepatocellular carcinoma
HDP(s)	Host-defence peptide(s)
Hz	Hertz
IDM	Intensified disease management
Ile (I)	Isoleucine
IM	Intramuscular
IV	Intravenous
kHz	Kilohertz
LCP	Left circular polarised
Leu (L)	Leucine

LPS	Lipopolysaccharide
LTA	Lipoteichoic acid
LUV(s)	Large unilamellar vesicle(s)
Lys (K)	Lysine
MBC	Minimal bactericidal concentration
MDA	Massive drug administration
mdeg	Millidegrees
MDR	Multidrug resistance
Mg^{2+}	Magnesium ion
MH	Mueller-Hinton
MIC	Minimum inhibitory concentration
μg	Microgram
μl	Microliter
μm	Micrometre
μM	Micromolar
MLV(s)	Multilamellar vesicle(s)
ml	Millilitre
mm	Millimetre
mM	Millimolar
min	Minutes
N	Amine group
NAD^+	Oxidised nicotinamide adenine dinucleotide
NADH	Reduced nicotinamide adenine dinucleotide
nm	Nanometre
nM	Nanomolar
N/m	Newton metre
NMR	Nuclear magnetic resonance
NTD(s)	Neglected tropical disease(s)
PBS	Phosphate-buffered saline
PC	Phosphatidylcholine
PCT	Preventive chemotherapy and transmission
PE	Phosphatidylethanolamine

PEM	Photoelastic modulator
PG	Phosphatidylglycerol
pI	Isoelectric point
PLL	Poly-L-lysine
PMS	Phenazine methosulphate – Electron coupling agent
POPC	1-palmitoyl-2-oleoyl-glycero-3-phosphocholine
POPG	1-palmitoyl-2-oleoyl-sn-glycero-3-phospho-(1'-rac-glycerol)(sodium salt)
Pro (P)	Proline
PS	Phosphatidylserine
RCP	Right circularly polarised
RPMI	Roswell Park Memorial Institute
Rq	Surface roughness
res	Residue
s	Second
SD	Standard deviation
Ser (S)	Serine
TDB	Trypanosome dilution buffer
Thau-3	Thaulin-3
Thr (T)	Threonine
Tyr (Y)	Tyrosine
UV	Ultraviolet
Val (V)	Valine
VSG	Variant-surface glycoprotein
WHO	World Health Organisation
wt	Wild type
WTA	Wall teichoic acid
XTT	3´-[1-(phenylaminocarbonyl)-3,4-tetrazolium]-bis (4-methoxy6-nitro) benzene sulfonic acid hydrate

1 Introduction

1.1 Multidrug resistance – a current issue

Multidrug resistance (MDR) is a problem that affects populations worldwide. Stemming from complex and multifactorial events, it can be found anywhere we look, from hospital-acquired infections, to difficulty in treating cancers with chemotherapy and even in agriculture.

Antibiotic resistance is almost as old as the discovery of penicillin, with some believing it is older and an intrinsic factor present in the genome of bacteria, especially considering that *Staphylococcus* resistance to penicillin was identified three years before the production of the first antibiotic becoming widespread in 1943 [1]. Even though bacteria show a predilection to develop resistance to antibiotics, there seems to be little doubt that this predisposition has been exacerbated by the introduction of antibiotics, their widespread availability and misuse in both human and veterinary settings [1,2] (Table 1), giving rise to more virulent and resistant bacteria. Concerns relating to antibiotic resistance continue to grow in the present day, with existing antibiotics becoming increasingly useless against quickly adaptable pathogens and the inability of researchers and pharmaceutical companies in maintaining the pace of antibiotic discovery, so much so that in 2016 the World Health Organisation (WHO) was mandated by its member states to create a list of priority antibiotic resistant pathogens posing the greatest risk to human health in order to direct future research and development of new drugs [1–3].

Antibiotic	Year of market introduction	Year resistance identified	Resistant bacteria identified
Penicillin	1943	1940	*Staphylococcus*
Methicillin	1960	1962	*Staphylococcus*
Ceftazidime	1985	1987	Enterobacteriaceae
Levofloxacin	1996	1996	Pneumococcus
Linezolid	2000	2001	*Staphylococcus*
Ceftaroline	2010	2011	*Staphylococcus*

Table 1. Timeline of resistance developed for some antibiotics [4]

Amongst others, this list includes the so-called *ESKAPE* pathogens (*Enterococcus faecium*, *Staphylococcus aureus*, *Klebsiella pneumoniae*, *Acinetobacter baumanii*, *Pseudomonas aeruginosa*, and *Enterobacter spp.*) alongside other MDR Enterobacteriaceae (including *Escherichia coli*) [3] which have become genetically talented at employing a multitude of very successful mechanisms to avoid antibiotic action – antibiotic inactivation by irreversible enzymatic cleavage of the active compound, drug target site modification, increased efflux capability or low permeability of the drug as well as the ability to form biofilms that act as a barrier between the pathogen and antimicrobial agents protecting antibiotic tolerant dormant cells that go on to cause further infections [5].

Hand in hand with antimicrobial resistance walks the global rise in cancer related deaths. In many cases, to remove a tumour, surgery is an inevitable procedure and this is accompanied by the risk of picking up an infection during operation [6]. Thus, and taking into consideration the rise in MDR pathogens, the future of cancer patients seems to be going from bad to worse.

Additionally, if MDR becomes the norm, other forms of cancer treatment would forever become associated with risks such as bone marrow transplants where both patients and donor would risk contracting a MDR pathogen [6]. Not even treatments that are non-surgical would escape the scope of MDR if we take into account that chemotherapy and radiotherapy exert a deleterious effect not only against cancer cells but also on the immune system, weakening it and leaving patients vulnerable to infection by opportunistic pathogens [6].

Sadly for cancer patients worldwide, there are other issues that need to be urgently addressed in matters of cancer treatment with the most pressing probably being chemotherapy resistance. Presently, chemotherapy remains one of the most common treatments for cancer [7]. This usually means a cocktail of anticancer drugs that can include natural products, DNA-alkylating agents, hormone antagonists/agonists and antimetabolites which preferentially, but not exclusively, target rapidly dividing cancer cells and their proteins or receptors. However, there is evidence that cancer cells that underwent the first round of chemotherapy can develop acquired resistance upon relapse and that some types of cancer are actually naturally resistant to start with, as in they show intrinsic resistance to chemotherapy [8–10]. Hepatocellular carcinoma (HCC) is an

example of a type of cancer that killed more than 700 thousand people worldwide in
2012. It exhibits intrinsic resistance to chemotherapy through the expression of complex
mechanisms such as reduced drug uptake, enhanced drug efflux, reduced intracellular
drug concentration due to metabolism of active agents by the cancer cells, enhanced
repair of drug-induced modifications and modifications in the molecular targets of the
anticancer drugs [11].

It is clear to see how MDR spans across different types of diseases, bringing forward a
bleak vision of the future in matters of global healthcare unless new ideas and solutions
are brought forward. The need for new therapies that are faster acting, more effective,
safer, less toxic and that break away from the dogma of conventional compounds has
never been more urgent than now.

1.2 Neglected tropical diseases (NTDs) – African trypanosomiasis

Neglected tropical diseases or NTDs represent a group of infections that can be caused
by bacteria, viruses, parasites and fungi that are prevalent in many tropical and sub-
tropical developing countries where poverty is widespread [12] (Figure 1).
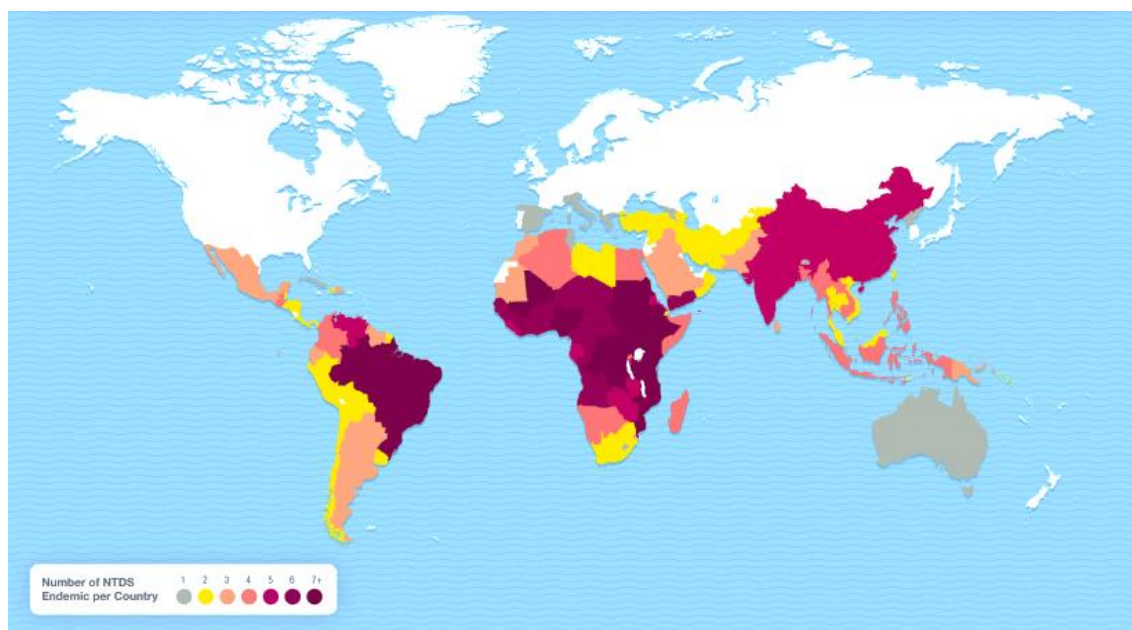

Figure 1. Burden of neglected tropical diseases map [13]. This map highlights endemic countries for ten NTDs
based on 2009-2010 data and international borders.
(Adapted from Uniting to Combat NTDs, 2017)

According to the World Health Organisation (WHO), more than 1 billion people worldwide are affected by NTDs [14]. This places a strain on developing economies and contributes to a cycle of poverty since it is extremely difficult for infected individuals to lead a productive life due to social stigma, discrimination and physical disabilities. Yet, many NTDs are preventable and could even be eliminated if the right steps were taken such as vector control measures, improved sanitation and mass prevention chemotherapy.

In 2012, international organisations that included the WHO and the Bill and Melinda Gates Foundation, met in London and set out goals to promote the control and potential elimination or eradication of a group of 17 NTDs [15]. To help establish those goals the WHO separated NTDs into two action groups: preventive chemotherapy and transmission control (PCT) NTDs and innovative and intensified disease management (IDM) NTDs.

The PCT group includes NTDs that can be controlled through the periodic administration of drugs that are usually efficient, safe and inexpensive to the entire population at risk – mass drug administration (MDA); while NTDs belonging to the IDM group rely on individual case finding and management due to the lack of appropriate tools for large scale use and this includes NTDs such as human African trypanosomiasis (HAT) [16].

African trypanosomiasis (AT) is an insect borne parasitic disease caused by several different species and subspecies of salivarian trypanosomes whose life cycle comprises of infecting their tsetse fly vector and subsequently mammalian hosts. The subspecies *T. b. rhodesiense* and *T. b. gambiense* cause HAT (Figure 2), also known as sleeping sickness, while *T. b. brucei* is amongst the most relevant subspecies that cause animal trypanosomiasis or nagana in other mammals, such as cattle and house pets, and in rare occasions has also been reported to infect humans [17,18]. If left untreated these infections usually lead to death and huge economic damages due to the loss of livestock.
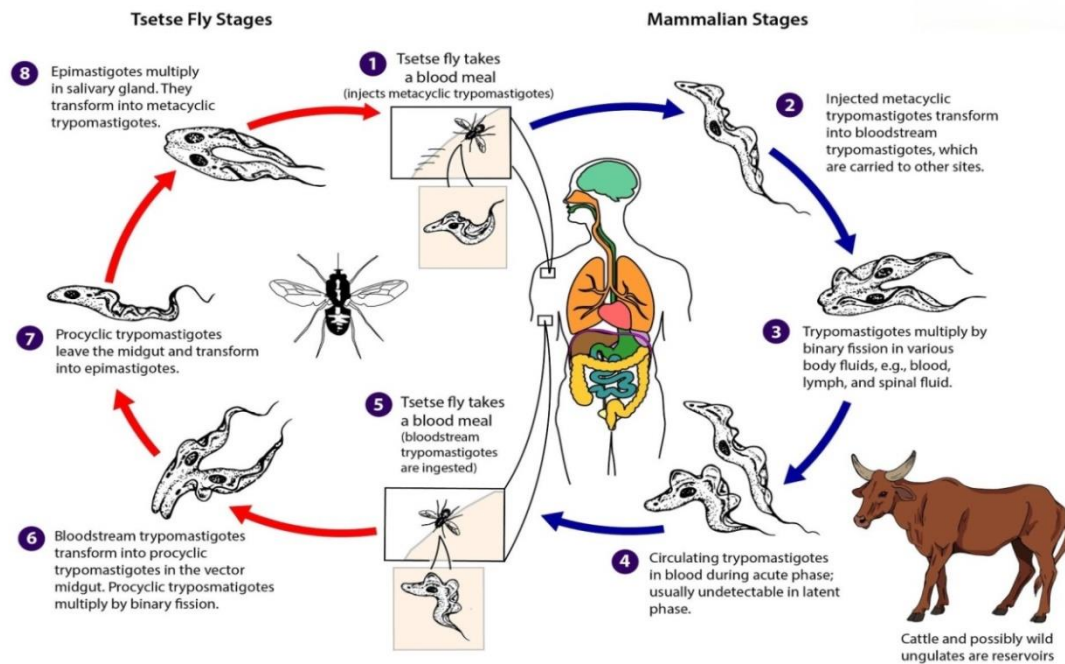
Figure 2. Human African trypanosomiasis life cycle [19]**. S**ubspecies *T. b. gambiense* and *T. b. rhodesiense* are morphologically indistinguishable and cause distinct disease patterns in humans: chronic West African trypanosomiasis and acute East African trypanosomiasis respectively. The third subspecies *T. b. brucei* primarily infects cattle and under normal conditions does not infect humans.
(Adapted from Centers for Disease Control and Prevention, 2019)

Diagnosis of HAT can be difficult and is not straightforward since it depends on patient's history, which subspecies is causing it as well as the stage of the infection. Usually the primary diagnostic test is a thin or thick peripheral blood smear to visualise the parasite. In the case of *T. b. rhodesiense* this works quite well due to the associated high levels of parasitaemia, however, the same does not apply to *T. b. gambiense* which presents with cyclical parasitaemia leading to intermittent high blood parasite levels [20]. Determining the stage of the infection can also be a challenge due to a lack of objective criteria to differentiate early-stage disease from late-stage, nevertheless the currently accepted identifier of late-stage infection for both types of HAT is an examination of the cerebrospinal fluid (CSF) performed by lumbar puncture to prove that the parasites have crossed the blood-brain barrier (BBB) and are invading the central nervous system (CNS) [20].

Pharmacological treatment for both HAT variants presents with toxicity, especially for late-stage disease, and can be painful since all treatments must be administered

intravenously or intramuscularly (Table 2), not to mention the fact that some of the medication used present serious side effects which might occasionally lead to death [21,22].

	First-line treatment	Second-line treatment
Early stage		
T. b. rhodesiense	Suramin (IV)	Pentamidine (IM)
T. b. gambiense	Pentamidine (IM)	Suramin (IV)
Late stage		
T. b. rhodesiense	Melarsoprol (IV)	None available
T. b. gambiense	Eflornithine (IV) plus nifurtimox (oral)	Melarsoprol (IV)

Table 2. Drugs used in treatment of human African trypanosomiasis [23]. IV – intravenous; IM – intramuscular.

Concerted efforts by international organisations and governments has led to a decrease in the number of cases per year of HAT in endemic areas, however, eradication of the disease requires continuous and prolonged vector control, is heavily dependent on a differential and correct diagnostic and the current drugs used in treatment not only can be toxic but also require specialised personnel to administer them, which might involve a long trip to the nearest health centre for many of those affected. Therefore, new pharmacological solutions to fight this disease would be welcome, especially if they translated into effective, quick and easy to distribute and administer medication.

1.3 Host-defence peptides (HDPs)

The emergence and dissemination of MDR in pathogens and in disease, alongside an international desire to combat NTDs in some of the poorest countries in the world, has driven researchers to look into new types of antimicrobial agents [24] such as host-defence peptides (HDPs).

HDPs, also known as antimicrobial peptides (AMPs), are produced by all known living species, playing a role in innate immunity, and were first discovered in the 80s as naturally occurring polypeptide sequences of about 12 – 50 residues that demonstrated antimicrobial activity, were gene-encoded and derived from precursor peptides [24–26]. In addition to being usually short, HDPs are commonly cationic and amphipathic and this allows them to accumulate and acquire specific three dimensional structures upon contact with polyanionic cell surfaces, such as the ones belonging to Gram-negative and

Gram-positive bacteria, that contain acidic polymers like lipopolysaccharides and teichoic acids [26]. More recent research described some AMPs that also possessed anticancer properties and were thus labelled as anticancer peptides (ACPs) [27]. This should come as no surprise when considering that AMPs mode of action appears to rely on initial electrostatic interactions between the peptides and anionic membranes, so while healthy cells contain the negatively charged phospholipid phosphatidylserine (PS) hidden in their plasma membrane's inner-leaflet, cancer cells on the other hand show a more disordered arrangement between inner and outer cell membrane leaflets which leads to PS being exposed in the outer leaflet and so bestowing a negative charge to cancer cell membranes that would attract ACPs [8,28] (Figure 3).
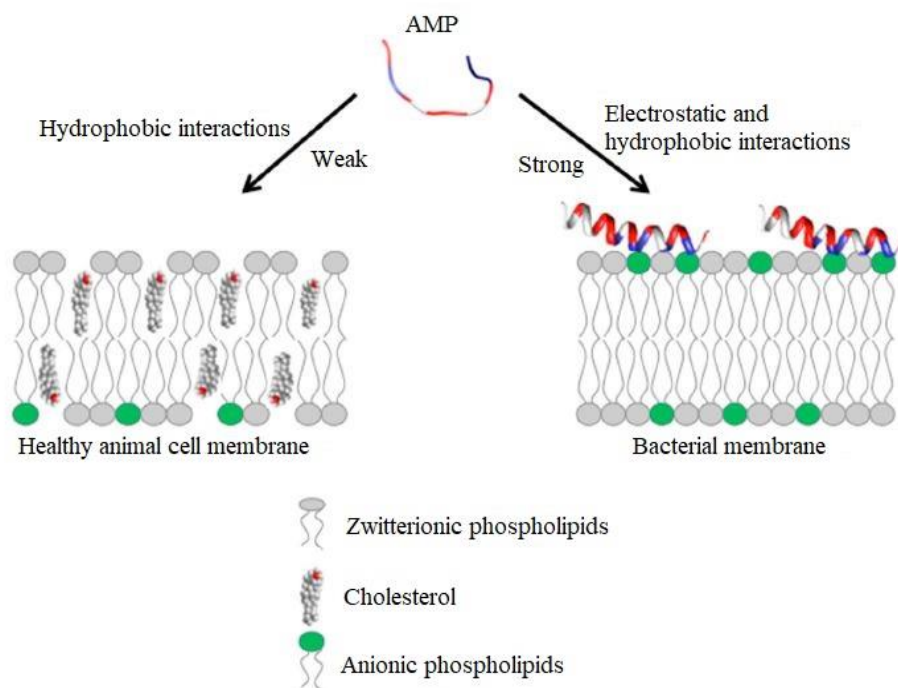
Figure 3. Interaction of cationic AMPs with healthy animal membranes and bacterial membranes [29]
Similarly to bacteria, cancer cell membranes also display a negative charge due to the presence of anionic phospholipids on the membrane's outer leaflet. (Adapted from Kumar, 2018)

1.3.1 Common mechanisms of action

Several models of action that rely on the initial electrostatic and hydrophobic interactions have been described for AMPs. The basis is that AMPs gather and self-assemble on the bacterial membrane creating an AMP "carpet" (the carpet model) or a transmembrane pore (barrel-stave pore and toroidal pore models) [30].

In the carpet model AMPs swamp the bacterial membrane forming a carpet-like structure that adsorbs parallel to the lipid bilayer until the surface of the membrane is covered, resulting in a unfavourable environment that leads to membrane disintegration in a detergent-like effect [26,30] (Figure 4c).

In pore-forming models like the barrel stave model, peptide to peptide interactions are essential. In order for that to occur, AMPs initially orientate themselves parallel to the bacteria membrane so as to eventually insert perpendicularly into the lipid bilayer, promoting peptide to peptide interactions similar to the ones seen in membrane protein ion channels and eventually membrane depolarisation and cell death take place [30] (Figure 4a). The toroidal pore model is somewhat similar to the barrel stave model with the exception that peptide to peptide interactions do not occur and are instead replaced with the formation of a pore that is partially peptide and partially phospholipid headgroup belonging to the lipid bilayer of the bacterial membrane [30,31]. The characteristics of the toroidal pore allow for peptide translocation into the bacterial cytoplasm which may potentially lead to the targeting of intracellular components [30,31] (Figure 4b).

However, the action of peptides cannot always be explained by the disruption of membranes and AMPs have been reported to be able to target other processes like the pathogen's metabolism or cell division [8]. ACPs have also shown differentiated modes of action ranging from the activation of apoptosis signalling to the recruitment of immune cells to attack cancer cells [8].
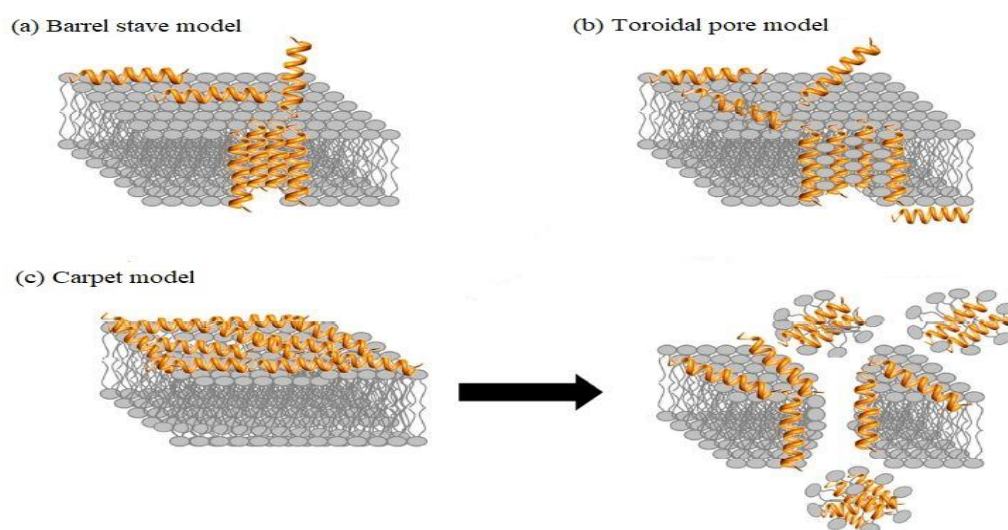

Figure 4. Proposed mechanisms of action for AMPs in bacteria [29]. (Adapted from Kumar, 2018)

1.3.2 HDPs from Patagonian amphibians – their importance and characterization

To date, more than 3000 HDPs from various origins with a wide range of activities have been listed on the antimicrobial peptide database (APD) and of those more than 1000 originate from amphibians, mainly frogs [32], meaning that frog-related HDPs account for roughly 33% of all active antimicrobial peptides in the APD. Frog skin HDPs have been reported as being highly potent against antibiotic-resistant bacteria, yeasts, protozoa and fungi due to their ability to permeate and destroy their target's plasma membrane or by inactivating intracellular targets [27]. Each frog species expresses its own stock of AMPs through prepropetides harbouring a conserved signal peptide, an acidic propiece and a highly variable domain that encodes for the AMPs that form a distinct marker for each amphibian specie [27,33]. Within each species repertoire of AMPs we can find different sequences, sizes and varying spectrums of action, yet, in the midst of all this variability many peptides share common features across frog species and therefore have been classified into peptide families like the dermasemptins, magainins and temporins [27,33]. This rich variability has turned the spotlight onto the potential industrial applications of skin secretions from amphibians and the Patagonian region alone has more than 50 unexplored species [33] making it an attractive target for HDP research, alongside other nations like Brazil and Costa Rica.

Recent studies by our Argentinian partners identified Thaulin-1, the first antimicrobial peptide with activity against *E. coli* isolated from the skin of a Patagonian frog *Pleurodema thaul* [33]. Ongoing research is currently looking at HDPs secreted by the skin of other Patagonian species from which the peptides assessed in this thesis have originated from (Table 3 and Table 4). According to the data collected by our collaborators, Thaulin-3 (Thau-3) [33], PSo-7, PSo-4 and PSo2-2 have been identified in frogs from the *Pleurodema* genus, while Ooc-1 originated from the *Odontophrynus occidentalis* frog.
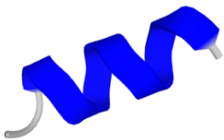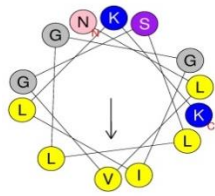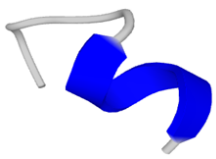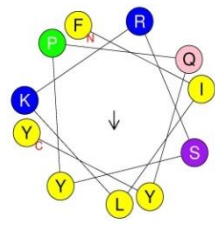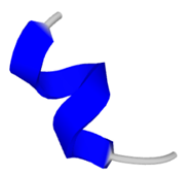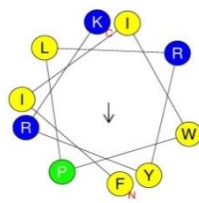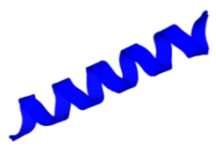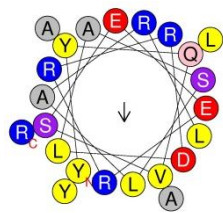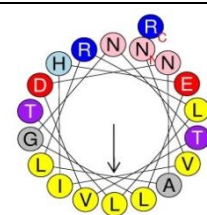
Peptide name	Sequence	Charge	Predicted 3D Structure	Schiffer and Edmundson wheel projection diagrams
Thaulin-3	N**LV**GS**LL**GG**IL**KK	+2		
PSo-7	**FIL**KRSY**P**QYY	+2		
PSo-4	**FII**WP**L**RYRK	+3		
PSo2-2	YYQ**V**SEERRRD**LAS LAR**LY **ALA**R	+2		
Ooc-1	N**VI**HE**LG**NT**V**DN**AL**R**LL**TR	0		

Table 3. New uncharacterized HDPs extracted from skin secretions of Patagonian amphibians by a partner lab and their predicted characteristics. Peptide sequence residues in dark red and bold = hydrophobic amino acid residues; underlined, dark red and bold residues = hydrophobic amino acids predicted to be on the same surface. Amino acid colour code for wheel projection diagrams: yellow = non-polar/hydrophobic (Leu, Val, Tyr), grey = Gly, Ala, blue = basic (Lys, Arg), purple = polar without charge (Thr, Ser), pink = polar without charge (Asn, Gln), green = Pro. The arrows represent the helical hydrophobic moment. Apart from Thau-3 [33], the data on the remaining peptides has never been published. The work on this table was carried out by Lorena Cancelarich, PhD student, from Mariela M. Marani's lab at IPEEC-CONICET.

	Thaulin-3	PSo-7	PSo-4	PSo2-2	Ooc-1
Theoretical isoelectric point (pI)	10	9.53	11	9.69	6.75

Table 4. Theoretical isoelectric point for Patagonian amphibians' derived peptides. Most of these peptides would require an alkaline environment to become electrically neutral, with the exception of Ooc-1 which has an ever so slightly acidic pI. Apart from Thau-3 [33], the data on the remaining peptides has never been published. The work on this table was carried out by Lorena Cancelarich, PhD student, from Mariela M. Marani's lab at IPEEC-CONICET.

Frog skin AMPs with lytic activity seem to share common traits such as the presence of basic amino acids that confer a net positive charge, high content of hydrophobic amino acids and an inclination to form amphipathic α-helix or β-sheet structures [27]. Also, research implies that certain amino acid residues, and the position they occupy in the peptides sequence especially in the N and C terminus, might help predict their antimicrobial capacity, as well as the fact that in general antibacterial peptides tend to have higher portions of cysteine (C), lysine (K), glycine (G) and isoleucine (I) when compared to non-antibacterial peptides [33,34]. Even though peptides Thau-3, PSo-7, PSo-4, PSo2-2 and Ooc-1 show most of the characteristics inherent to active AMPs, they showed none to very weak activity (except for Ooc-1 which was never assessed) when tested against Gram-negative and Gram-positive bacteria by our partners. However, these peptides were never assessed for potential anticancer and antiparasitic activity, in fact Ooc-1 properties had never been studied, and yet they seemed to possess all the right characteristics with some showing similarities, in matters of structure, with other active HDPs listed in the APD that show anticancer activity. Therefore, these peptides were the perfect candidates to undergo further study and characterisation as part of this project.

1.4 Some available tools used to study peptide action and structure

When it comes to the study of peptides, there is an array of options available depending on the main objective of our research. In this section we briefly highlight the principles behind the tools we decided to employ in studying the action and structure of our Patagonian amphibians' derived peptides.

Minimum inhibitory concentration (MIC) assays are widely used in antimicrobial susceptibility testing and are considered the "gold standard" in determining the susceptibility of organisms to antimicrobials [35]. MICs are defined as the lowest

concentration of an antimicrobial which prevents visible growth of a microorganism after the appropriate incubation period and determined by agar dilution or broth dilution where the microorganism is incubated in increasing concentrations of the antimicrobial compound.

Minimal bactericidal concentration (MBC) is also a helpful tool to assess the bactericidal capacity of antimicrobials unveiling the lowest concentration necessary to prevent growth of a microorganism after subculture onto antibiotic-free media [35] and how close that concentration is to the MIC.

Atomic force microscopy (AFM) is a high resolution scanning probe microscopy, able to reach atomic and molecular resolution, with the capacity of imaging in air or in liquid, nonconductive and conductive surfaces beyond the light diffraction limit [36] allowing us to study sample topography and, in this instance, evaluate possible damage caused to bacterial cell wall by our peptides. The AFM technique consists of scanning the specimen's surface with a sharp tip (probe) mounted on a flexible cantilever. Depending on the type of sample or parameters being analysed, the AFM can be operated in two modes: static mode or dynamic (AC or intermittent contact) mode. For the purpose of our analysis the intermittent contact mode was used where the cantilever is oscillated close to the resonance frequency set by the user. The tip-sample repulsion at the atomic level is transduced into changes of the motion and deflection of the cantilever and by an optical lever mechanism, in this way a height value is linked to each position on the *x,y* plan, and thus, resulting in a pseudo-three-dimensional (3D) image of the sample's surface [36,37] (Figure 5).
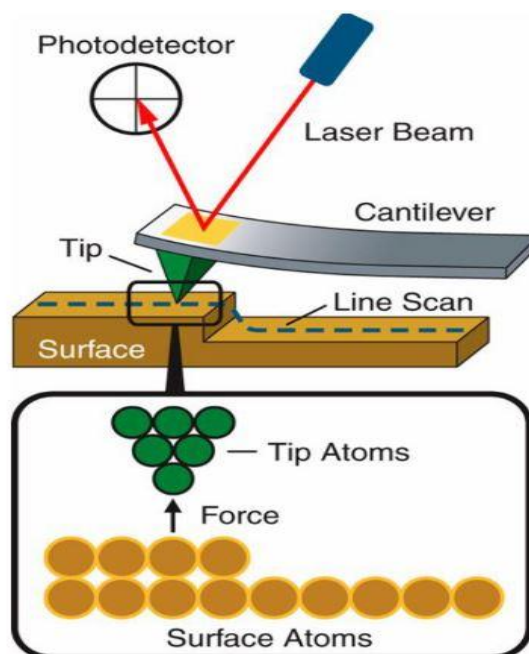
Figure 5. Scheme of a measurement with AFM [38]. The tip is brought into a few nanometres from a sample surface, forces between the tip and the sample originate deflections of the cantilever which are measured using a laser beam that reflects on the cantilever and is collected by a four sectors photodetector. The tip is mounted on a piezoelectric system responsible for scanning in the x, y and z directions.

Colorimetric and fluorometric indicators are commonly used in assays for the quantification of cell proliferation, viability and metabolism, thus are very useful tools when studying the effect new peptides may exert on cells, protozoan parasites and even fungi. Popular non-radioactive colorimetric indicators include the water-soluble sodium 3´-[1-(phenylaminocarbonyl)-3,4-tetrazolium]-bis (4-methoxy6-nitro) benzene sulfonic acid hydrate, also known as the tetrazolium salt XTT. This yellowish salt forms a bright orange formazan compound when reduced at the cell surface by trans-plasma membrane electron transport, via the 1-methoxy PMS carrier, from intracellular NADH produced by metabolic active cells [39,40] (Figure 6) and the changes in absorbance can be quantified by a spectrophotometer.
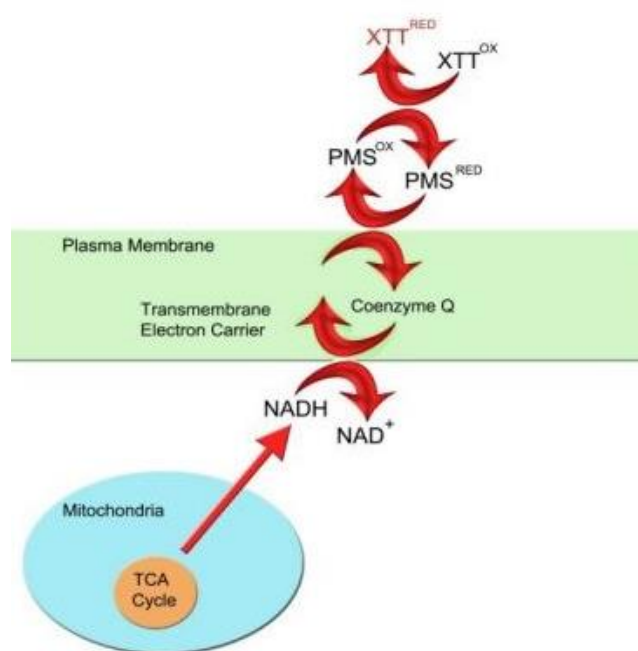
Figure 6. The colorimetric reduction of XTT [41]

AlamarBlue is another non-radioactive, water-soluble, non-toxic indicator that can be used in cell viability studies [42]. It is stable in culture medium and permeable through cell membranes, hence, it is capable of monitoring the reducing environment of living cells [42]. Its active compound, resazurin, can be reduced by mitochondrial-reductases, cytochromes and other enzymes present in the cytoplasm. Resazurin is pink and highly fluorescent, and thus can be used in both colorimetric and fluorometric assays and assessed by a spectrophotometer or fluorometer respectively [42]. In this project we employed the fluorescence characteristics of alamarBlue to assess cell viability.

Peptide aggregation is a common occurrence and it can influence the physical stability, activity, toxicity and immunogenicity of a peptide [43–45]. 8-anilino-1-naphthalenesulfonic acid or ANS is frequently used as a probe in fluorescence studies of proteins or peptides due to its sensitivity to the polarity of its microenvironment [46]. It non-specifically interacts with so called hydrophobic pockets that originate from peptide aggregation increasing the probe fluorescence emission maximum resulting in a blue shift and intensity increase [47], this translates into an increase of frequency and energy while wavelength decreases.

Circular dichroism (CD) is a method that, among other things, can be used to provide a

quick determination of the secondary structure of peptides, how they interact with their
environment in matters of conformational changes, peptide folding and binding [48]. It
benefits from the fact that multiple samples can be measured in a few hours and it only
requires small amounts of peptide in solution. CD is an absorption spectroscopy method
based on the principle that light can be circularly polarised in two directions: left and
right [49] (Figure 7). Optically active chiral molecules may absorb right circularly
polarised (RCP) and left circularly polarised (LCP) light to different extents and
produce different refraction indices and amplitudes for the two waves thus resulting in
an elliptically polarised wave [49,50] (Figure 8).
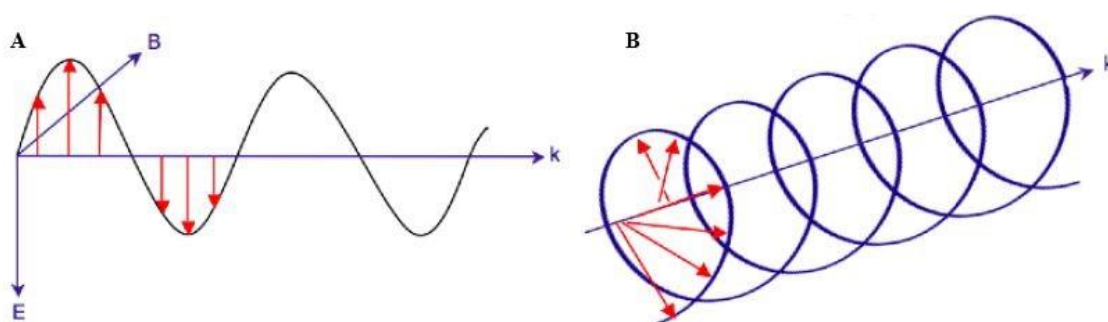
Figure 7. Diagram of linearly polarised and circularly polarised light [51]. Most light sources emit waves of
magnetic and electric fields oscillating in all directions perpendicular to the propagation vector. When the electric
field vector oscillates in only one plane while variating in magnitude the result is linear polarised light (**A**),
whereas circularly polarised light (**B**) occurs when the vector direction varies while it rotates around the
propagation axis but the magnitude remains constant.
(Adapted from Wikipedia, 2019)
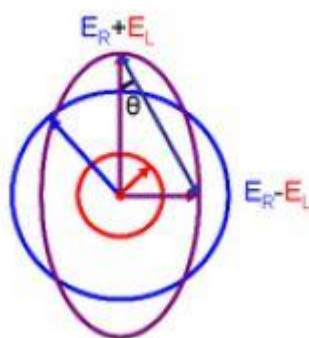
Figure 8. Elliptically polarised light [52]. Represented in purple is the elliptically polarised light which results from
the superposition of RCP (blue) and LCP (red) light. E is the magnitude of the electric field vector and the degrees of
ellipticity (θ) are given by the angle of E at its maximum and minimum.

In 1960, French scientists Grosjean and Legrand introduced the electro-optical modulation techniques in which most CD instruments are still based on to this day [53] (Figure 9). A CD spectrum is generated when the dichroism is measured as a function of wavelength (λ) [49]. The far-ultraviolet (UV) CD spectra ($\lambda = 260 - 180$ nm) is commonly used to study peptide conformation as peptide (amide) bonds are the most absorbing components in that region.
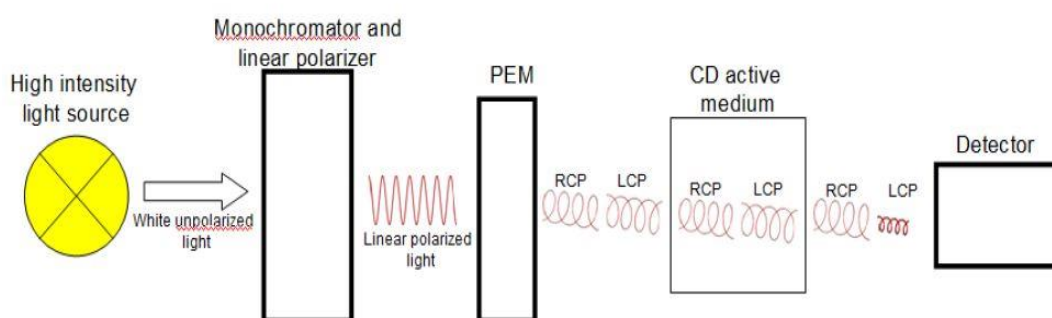
Figure 9. Instrumentation schematics for a common CD spectrometer [54]. White light is linearly polarised after passing through a monochromator and subsequently transformed into circular polarised light by a photoelastic modulator (PEM). Samples are subjected to incident light that switches between RCP and LCP which causes absorption changes and therefore the different molar absorptivity can be calculated and is usually reported in terms of θ.

Common secondary structures include α-helix, β-sheet and random coil and the resulting spectrum will be particular to a specific secondary structure [55] (Figure 10).

The far-UV CD spectrum for α-helix is probably the most intense and distinctive amongst all secondary structures. Characterised by two negative maxima around 222 nm and 208 nm (although these might vary slightly depending on the characteristics of the α-helix), crossing over to positive at around 200 nm to exhibit a positive band near 192 nm [56]. β-sheet CD spectra can somewhat vary depending on the β conformation which can be single strand, parallel, antiparallel or barrel. The spectrum shows a red-shift in relation to an α-helix where it crosses from negative to positive and it displays a single negative band at around 217 nm as well as a single positive band near 200 nm [56]. The dominant feature in random coil spectra of small peptides tends to be a pronounced negative band nearby 200 nm and sometimes a weak positive band can be seen near 220-230 nm [56].
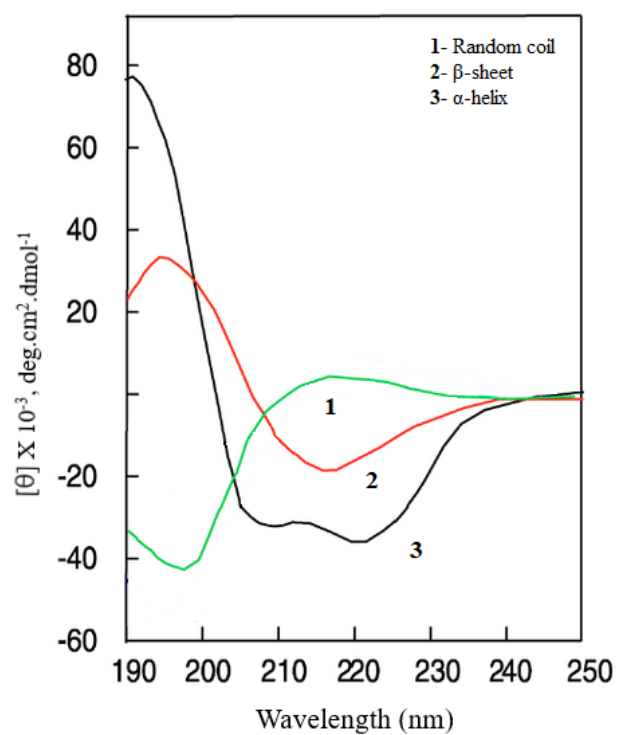
Figure 10. Circular dichroism spectra of proteins and peptides with representative secondary structures [57]
(Adapted from Greenfield, 2006)

1.5 Aims and objectives

This project aims to explore and highlight the anticancer, antibacterial and antiparasitic properties of Argentinian amphibians' derived peptides PSo-7, PSo-4, PSo2-2, Thaulin-3 and Ooc-1. It is intended that the research findings will contribute towards the work already being developed by partner labs in South America and that it will open a path to possible pharmacological development of new drugs.

The above aims raise the following core project objectives:

- To identify the antibacterial capacity of peptide Ooc-1, on Gram-negative and Gram-positive bacteria, as well as to gauge the action of Ooc-1 and PSo-4 on the bacterial cell wall;
- To evaluate if any of our chosen peptides exerts anticancer action on cells of human hepatocellular carcinoma;
- To investigate the potential of these peptides as antiparasitic drugs against the protozoa *Trypanosoma brucei brucei*.
- To study the behaviour, conformation and secondary structure of the peptides when in aqueous solution or in the presence of lipid vesicles and to assess the effect it might have on their scope of action.

2   Material and Methods

2.1   Bacteriological techniques

2.1.1 Bacterial strains and growth conditions

Escherichia coli (ATCC® 25922™) and *Staphylococcus aureus* subsp. *aureus* (ATCC® 25923™) were used for minimum inhibitory concentration (MIC) tests against peptide Ooc-1 (Appendix 1 and Appendix 2 respectively). Both strains are well known for their susceptibility to a variety of antibiotics and for their use as quality control strains [58][59].

Mueller-Hinton (MH) broth (Fluka® Analytical, Sigma-Aldrich, St. Louis, MO, USA) was routinely used for growth and MIC testing medium of *E. coli* and *S. aureus* while MH agar (VWR International, Leuven, Belgium) was employed for minimal bactericidal concentration tests (MBC), strain maintenance and storage. Both MH broth and agar were autoclaved before use (121ºC for 15 minutes).

E. coli and *S. aureus* stocks kept in long-term storage at -80ºC in 10% glycerol were thawed and 100 µl of each bacterium were pipetted into 50 ml Falcon tubes containing 5 ml of MH medium at room temperature. The inocula and respective negative controls (MH medium only) were incubated overnight at 37ºC, after which, the bacteria and controls were streaked onto sterile MH agar plates using the quadrant method and placed in incubation at 37ºC overnight and assessed for contamination the following morning.

Inoculated MH agar plates were stored in the fridge at 4ºC for no longer than 4 weeks. All procedures and experimental techniques in this project involving bacteria were performed in aseptic conditions.

2.1.2 Minimum inhibitory concentration (MIC) assays – Broth microdilution method

The broth microdilution method using MH medium was used for MIC determination of peptide Ooc-1 against the already mentioned *E. coli* and *S. aureus* strains (Figure 11) stored in MH agar plates at 4ºC.

Clinical Laboratory Standards Institute (CLSI) standards guidelines were followed for

inoculum preparation by direct colony suspension, microplate inoculation, incubation conditions and quality control [60] although some adjustments were made due to limited availability of Ooc-1 for preparation of intermediate dilutions.
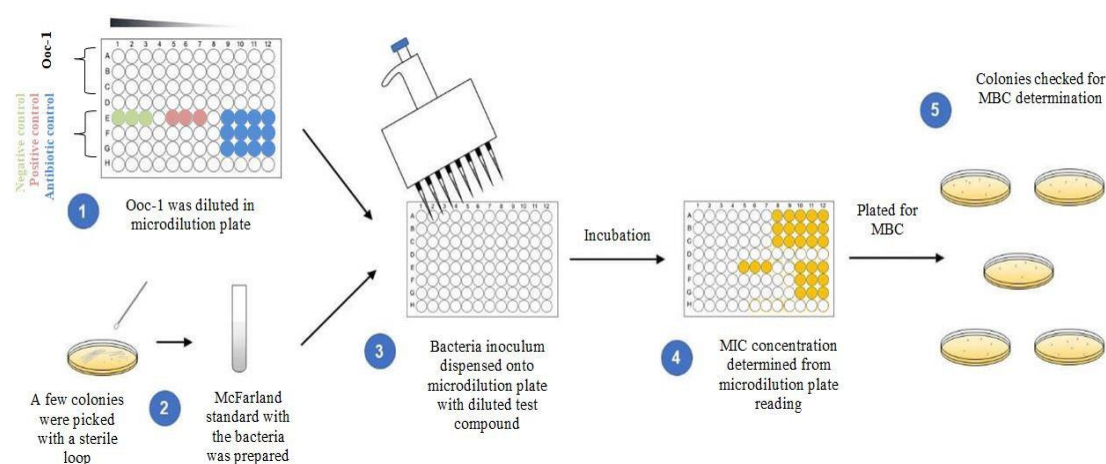
Figure 11. MIC determination of Ooc-1 against *E. coli* ATCC 25922 and *S. aureus* ATCC 25923 [61]**.** Antibiotic control wells for *E. coli* contained ampicillin whereas *S. aureus* antibiotic control wells had vancomycin. MH medium and PBS were pipetted into negative control wells while positive control wells were inoculated with MH medium, PBS and bacteria.
(Adapted from Emery Pharma, 2019)

Ooc-1 stock [5 mM] in 1µm filtered water (Sigma-Aldrich, St. Louis, MO, USA), kept at -20ºC, was diluted to intermediate concentrations 2.5 mM / 1 mM / 500 µM / 250 µM / 125 µM / 62.5 µM / 31.25 µM / 15.63 µM / 7.8 µM in sterile phosphate-buffered saline (PBS) solution (1X) pH 7.2 (Gibco, Paisley, UK) and stored in sterile low retention microcentrifuge tubes (Biotix, San Diego, CA, USA) at -20ºC.

Ampicillin sodium salt (Sigma-Aldrich, St. Louis, MO, USA) and vancomycin hydrochloride (Melford, Chelsworth, UK) were used as antibiotic controls for *E. coli* and *S. aureus* respectively. Stocks were prepared according to CLSI guidelines [60] and stored at -20ºC while intermediate dilutions were made fresh in MH medium at concentrations ranging from 40 µg/ml – 5 µg/ml for vancomycin and 140 µg/ml – 80 µg/ml for ampicillin.

One microplate of 96 clear, flat bottom wells (TPP, Trasadingen, Switzerland) was prepared for each organism. Microplate wells containing Ooc-1 were inoculated with 70 µL of MH medium, 20 µL of Ooc-1 intermediate dilutions and 10 µL of overnight incubated bacteria which were standardised in MH medium to 0.5 McFarland through

optical density readings by a spectrophotometer (Genesys 10-S, Thermo Fisher Scientific, Madison, WI, USA). The bacteria were then diluted to yield 1.5×10^4 CFU/well. Ooc-1 dilutions in microplate ranged from 500 µM/well to 1.56 µM/well. 80 µL of MH medium, 10 µL of ampicillin/vancomycin intermediate dilutions and 10 µL of bacteria were pipetted into antibiotic control wells with concentrations ranging from 14 µg/ml – 8 µg/ml of ampicillin/well and 4 µg/ml – 0.5 µg/ml of vancomycin/well. Negative control wells contained 80 µL of MH medium and 20 µL of PBS while positive control wells were inoculated with 70 µL of MH medium, 20 µL of PBS and 10 µL of bacteria.

Microplates were incubated for 20 h at 37ºC and MIC was determined as the lowest concentration that inhibited visible growth to the naked eye. Antibiotic controls were compared to EUCAST (2019) breakpoints [62].

After overnight incubation, the contents of Ooc-1 testing wells with MIC concentrations were streaked onto MH agar plates and underwent further overnight incubation at 37ºC to determine MBC.

MIC and MBC testing were performed twice; MIC samples were assayed in triplicate (1st assay) and in duplicate (2nd assay) owing to the limited availability of Ooc-1.

2.1.3 Bacterial cell wall assessment via AFM analysis

Samples used for AFM analysis originated from the MIC assays described in **2.1.2**. 80 µL droplets of test samples were applied onto 2 poly-L-lysine (PLL; Sigma-Aldrich, St. Louis, MO, USA) coated glass slides and allowed to stand at room temperature for 5 minutes (min). After deposition, all samples were rinsed 4 times with 1µm filtered water (Sigma-Aldrich, St. Louis, MO, USA), air-dried at room temperature and stored overnight in a desiccator.

AFM imaging was conducted using a JPK Nano Wizard IV (Berlin, Germany) mounted on a Zeiss Axiovert 200 inverted microscope (Jena, Germany). The device is used on top of an anti-vibration table, inside a homemade acoustic isolation hood.

Measurements were carried out in intermittent contact mode using uncoated silicon ACT cantilevers (Applied NanoStructure, Santa Clara, CA, USA) that have typical resonance frequencies of 200-400 kHz and a spring constant between 13-77 N/m.

On average, five individual bacterial cells were imaged for untreated controls

containing no peptide and for peptide concentrations from 1.8x < MIC to 5x < MIC at a
scan rate set to no less than 1 Hz. Medium only samples were also imaged to establish
background (Appendix 7).

Height and amplitude images were recorded and line-fitted as required with the image
analysis software Gwyddion. Roughness and cell height data were also acquired using
Gwyddion. Surface roughness (Rq) and cell height data for treated and untreated cells
(at 100 – 200 µM for Ooc-1 and at 75 – 100 µM for PSo-4) were averaged, plotted and
statistically analysed via a two-way analysis of variance (ANOVA) test using GraphPad
Prism 5. Experiments were replicated twice.

2.2 Parasitological techniques

2.2.1 Parasite strain and growth conditions

T. brucei brucei Lister 427 is a virulent lab strain, originally isolated in 1960 from an
early sheep infection in Uganda and transferred to the Lister Institute in London in 1961
[63][64]. The *T. b. brucei* 427 strain is a commonly used laboratory strain that has been
described as non-infectious to humans, unable to undergo development in the insect
vector and monomorphic [63]. This means that parasites from this strain mitotically
divide into long slender forms only, being unable to develop into any other form. More
information related to the history and lineage of the strain can be found elsewhere [65].

The choice of the Lister 427 strain for this project was due to the fact that it can be
used as a model for more dangerous strains such as *T. b. rhodesiense* or *T. b.
gambiense*. Another advantage is the fact that its growth is continuous and exponential
and *in-vitro* cultures do not require synchronisation since Lister 427 long slender
bloodstream forms cannot further develop into other bloodstream forms.

The Luísa Figueiredo Lab (*Instituto de Medicina Molecular, Faculdade de Medicina
da Universidade de Lisboa*) kindly donated wild type (wt) *T. b. brucei* 427 bloodstream
form (BSF) cells (Appendix 3) that were used in viability assays to assess the effect of
the amphibian peptides. These BSFs had been stored at -80ºC in 10% glycerol (Sigma-
Aldrich, St. Louis, MO, USA) and immediately after defrosting were maintained in log
phase growth in 25 cm² tissue culture flasks (Nunc, Thermo Fisher Scientific, Roskilde,
Denmark) by subculturing at 24 h intervals. Cells were grown in HMI-11 medium [66],

also supplied by Luisa Figueiredo's Lab (Appendix 5), supplemented with 1% penicillin/streptomycin (Lonza, Verviers, Belgium) and incubated in a CO_2 incubator at 5% CO_2 and 37ºC. Growth conditions were also in a CO_2 incubator at 5% CO_2 and 37ºC, with cells being subcultured at either 24 or 72 h intervals in antibiotic free HMI-11 medium.

All parasitological techniques and procedures were executed in sterility in a class II biosafety cabinet.

2.2.2 Parasite viability assay – spectrophotometric measurement of fluorescence produced by the reduction of alamarBlue

The alamarBlue assay was optimised for the parasite concentration to be used (Appendix 8), for this, *T. b. brucei* Lister 427 BSF were grown as described in **2.2.1** and counted in a neubauer chamber with a light microscope (Zeiss Primovert, Göttingen, Germany). BSF were diluted ten-fold for concentrations ranging from 10^1 to 10^6 BSF/ml, 100 µl of each concentration plus a medium only control (background) were pipetted in triplicate into a clear, flat bottom, 96 wells microplate (TPP, Trasadingen, Switzerland) and incubated for 22, 46 and 70 h at 5% CO_2 and 37°C. 10 µl of alamarBlue (Invitrogen, Eugene, OR, USA) were added to the appropriate wells and incubated for 2 h in a CO_2 incubator at 37°C. Each time point was analysed by a Tecan Infinite M200 (Tecan, Salzburg, Austria) microplate reader at $\lambda_{exc/em} = 530/590$ nm with a manual gain of 100. Data was corrected for background and this experiment was replicated twice.

AlamarBlue testing for BSFs subjected to the action of peptides followed the procedure established above with some minor changes. 90 µl of 5×10^4 BSF/ml were transferred into microplates alongside 10 µl of peptide intermediate stock, diluted in trypanosome dilution buffer (TDB), with concentrations ranging from 100 to 1.56 µM/well for all peptides. Control (-) wells contained 10 µl of media instead of peptide, and 10 µl of 10% Triton X-100 were pipetted into control (+) wells. Wells containing media only were also included for background. Microplates were incubated for 70 h at which point 10 µl of alamarBlue were added and incubated at 5% CO_2 and 37°C for another 2 h. The Tecan Infinite M200 (Tecan, Salzburg, Austria) was used for fluorescence analysis, with the same settings already mentioned above, and a quick

inspection of the microplates was done under a light microscope (Zeiss Primovert, Göttingen, Germany). Results were corrected for background and normalised to control (-) values. Due to the small amount of peptides available as well as several problems with recurrent contaminations in the lab, we were only able to run this assay once.

2.3 Cell biology techniques

2.3.1 Cell line and culture conditions

Huh-7 is a well differentiated human hepatocellular carcinoma cell line established in 1982 from a liver tumour in a 57 year old Japanese male [67]. Epithelial-like and immortal, Huh-7 are adherent cells that tend to grow in flasks or plates as monolayers or multilayered islands depending on the availability of serum in the medium [68].

Huh-7 cells used in this project (Appendix 4) were generously donated by Diana Fontinha, PhD, from Miguel Prudêncio Lab (*Instituto de Medicina Molecular, Faculdade de Medicina da Universidade de Lisboa*) and were kept in storage at -80ºC in 10% DMSO (Merck, Darmstadt, Germany). Once defrosted cells were grown in modified RPMI-1640 medium (Appendix 6) supplemented with 10% of foetal bovine serum, 1% of non-essential amino acids and 1% penicillin/streptomycin, seeded into 25 cm^2 tissue culture flasks (Nunc, Thermo Fisher Scientific, Roskilde, Denmark) incubated in a CO_2 incubator at 37°C and 5% CO_2. Cells were checked under a light microscope (Zeiss Primovert, Göttingen, Germany) for growth and contamination and subsequently subcultured when 95% confluency was achieved in the tissue culture flask. Cell handling and related assays took place in a sterile class II biosafety cabinet.

2.3.2 Cell viability assay – spectrophotometric measurement of the absorbance produced by the cleavage of the XTT salt

For the optimisation of Huh-7 cell concentration and XTT incubation time to be used for this assay (Appendix 9), cells were grown as described in **2.3.1**, subsequently counted by a Moxi™ Z Mini Automated Cell Counter (ORFLO Technologies, Ketchum, ID, USA) and diluted ten-fold for concentrations ranging from 1 x 10^3 to 1 x 10^6 cells/ml. 100 µl of each concentration and a media only control were loaded in triplicate into a clear, flat bottom, 96 wells microplate (TPP, Trasadingen, Switzerland),

incubated for 24 h at 5% CO_2 and 37°C. The microplate was checked for cell adherence, growth and contamination under a light microscope (Zeiss Primovert, Göttingen, Germany) and allowed to incubate another 24 h. A cell proliferation kit (XTT) (Roche Diagnostics, Mannheim, Germany) was used to prepare the XTT reaction mix, according to the manufacturer's instructions [39], from which 50 µl were then immediately added to all appropriate wells in the microplate and incubated at 37°C and 5% CO_2 for 4, 6 and 8 h. Absorbance (*A*) for each time point was read by a Tecan Infinite M200 (Tecan, Salzburg, Austria) microplate reader at 492 nm and 690 nm (reference wavelength). Data was treated by applying the mathematical expression A_{492nm} - A_{690nm} and subtracting the media control (background). This assay was replicated twice.

The XTT assay followed the protocol described above with small modifications. 80 µl of Huh-7 cells at 5×10^4 cells/ml were pipetted into the microplate and incubated for 24 h. 20 µl of the PSo-4, PSo-7, PSo2-2, Thau-3 and Ooc-1 peptides intermediate stocks in PBS (1X) pH 7.2 (Gibco, Paisley, UK) were added to the cells in the appropriate wells in triplicate, producing concentrations ranging from 210 to 0.42 µM/well for PSo2-2 and 500 to 1 µM/well for the remaining peptides (this occurred due to an initial error with PSo2-2 stock concentration). 20 µl of media was added to the cells in the control (-) wells while control (+) received 20 µl of 10% Triton X-100 (Merck, Darmstadt, Germany). Wells containing media only were also included as a contamination control. Microplates were then again incubated for 24 h and subsequently the XTT mixture was added to the wells and left to develop for 4 h in the CO_2 incubator. Microplates were read as per the optimisation protocol described above and the results were treated by subtracting A_{690nm} from A_{492nm}, followed by the background and normalising to control (-). A two-way ANOVA test was used for the statistical analysis using GraphPad Prism 5. Three replicates of this experiment were carried out independently.

2.4 Structural characterisation of the peptides

2.4.1 Peptide aggregation studies with the fluorescent probe 8-anilino-1-naphthalenesulfonic acid

Peptide aggregation studies were carried out using PBS (1X) pH 7.2 (Gibco, Paisley,

UK) as a buffer, 25 mM of ANS (Sigma-Aldrich, St. Louis, MO, USA) solution was titrated with each of our amphibian peptides to yield final peptide concentrations between 20 µM and 500 µM. The peptides were previously diluted in PBS (1X) pH 7.2 (Gibco, Paisley, UK). Fluorescence emission spectra were collected for each sample between 400 nm and 650 nm, at an excitation wavelength (λ_{exc}) of 380 nm, in a Cary Eclipse fluorescence spectrophotometer (Mulgrave, Australia). Excitation and emission slits were set for 5 nm and 10 nm respectively, and scanning occurred at a rate of 225 nm/min. Two minutes were allocated to incubate each sample before measurement. For each spectrum obtained the fluorescence emission intensity (F_I) was corrected for background noise, dilution factor and normalised to the summation of F_I of the reference sample (ANS in PBS without peptide). The fluorescence emission intensity maximum (F_{Imax}) and wavelength of F_{Imax} (λ_{max}) were also recorded and individually plotted against peptide concentration. Measurements for all peptides were carried out on average three times on different days and statistical analysis was performed with GraphPad Prism 5.

2.4.2 Peptides' secondary structure analysis by CD

In order to analyse the secondary structure adopted by our peptides in buffer solution and possible conformational changes when exposed to negatively charged membranes, such as those of bacteria and cancer cells, we decided to use a lipid membrane model of large unilamellar vesicles (LUVs) made of a mix between 1-palmitoyl-2-oleoyl-glycero-3-phosphocholine (POPC) and 1-palmitoyl-2-oleoyl-sn-glycero-3-phospho-(1'-rac-glycerol)(sodium salt) (POPG) to mimic those conditions. In a chemical hood, 30 mM mixture of POPC and POPG (Avanti Polar Lipids, Inc. Alabaster, AL, USA) in a 1:1 ratio was prepared in chloroform (VWR International, Leuven, Belgium), and dried using a dry nitrogen stream to produce a lipid film which was left overnight in a vacuum system. The lipid film was hydrated with PBS (1X) pH 7.2 (Gibco, Paisley, UK) and subjected to 5 freeze/thaw cycles to produce multilamellar vesicles (MLVs). MLVs were extruded by hand 21 times through 0.1 µm pore size polycarbonate membranes mounted in a Mini-Extruder (Avanti Polar Lipids, Inc. Alabaster, AL, USA) previously conditioned with PBS.

CD measurements were carried out in a JASCO J-815 spectropolarimeter (Tokyo,

Antibacterial, antiparasitic and anticancer properties of host-defence
peptides from Argentinian amphibians
Material and Methods

Japan) with 1.0 mm path length cuvettes. Spectra were acquired at 25°C, between 200 and 260 nm, with a data pitch of 0.2 nm, wavelength sampling velocity of 200 nm.min^{-1}, 5 accumulations and data integration time of 1s. Three types of conditions were measured: PBS buffer titrated with lipid up to a final lipid concentration of 6.7 mM (Appendix 16), PBS buffer with 200 µM of peptide titrated with buffer to mimic lipid additions and PBS buffer with 200 µM of peptide titrated with lipid up to a final lipid concentration of 6.7 mM and peptide concentration of 152 µM. Spectra data was treated as described elsewhere [69] and visually analysed. All conditions were measured independently once due to time constraints and limited availability of peptides.

3 Results

3.1 None of the peptides show activity against *S. aureus* but Pso-4, PSo-7, Thau-3 and Ooc-1 exhibit antimicrobial properties against *E. coli* with Ooc-1 presenting bactericidal properties

Out of all tested peptides, PSo-4, PSo-7, Thau-3 and Ooc-1 displayed antimicrobial activity against *E. coli*, but none was able to have an effect on *S. aureus* (Table 5). PSo-4 exhibited the strongest activity while Ooc-1 showed bactericidal properties against *E. coli* at the MIC concentration of 500 µM (1073 µg/ml) (

Figure 12).

Peptide	*E. coli* ATCC 25922		*S. aureus* ATCC 25923	
	MIC (µg/ml)	MIC (µM)	MIC (µg/ml)	MIC (µM)
Thau-3 [**]	600	457	> 500	> 381
PSo-7 [**]	700	474	> 700	> 474
PSo-4 [**]	250	180	> 500	> 360
PSo-2.2 [**]	> 700	> 250	> 700	> 250
Ooc-1	1073	500	> 1073	> 500

Table 5. MIC results for Patagonian amphibians' derived peptides against the control strains of *E. coli* ATCC 25922 and *S. aureus* ATCC 25923. Values in bold highlight MICs for PSo-4, PSo-7, Thau-3 and Ooc-1. Apart from Thau-3 [33], the data on the remaining peptides has never been published. ** denotes the peptides whose MICs were performed by Lorena Cancelarich, PhD student, from Mariela M. Marani's lab at IPEEC-CONICET.
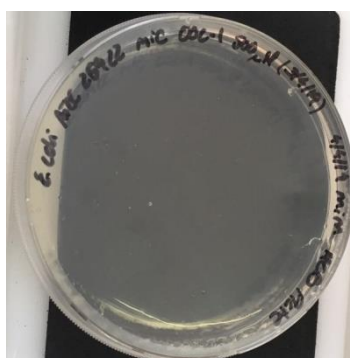

Figure 12. MBC for Ooc-1 at MIC of 500 µM. No visible growth was seen here meaning that there were no viable *E. coli* colony forming units after incubation with 500 µM Ooc-1.

This might indicate that PSo-4, PSo-7, Thau-3 and Ooc-1 action is concentration dependant and it is possible that it could rely on the interaction of these peptides with specific structures in the wall of the Gram-negative bacteria like *E. coli* as opposed to Gram-positive bacteria like *S. aureus*.

3.2 AFM analysis displays the effect of PSo-4 and Ooc-1 on *E. coli*'s cell wall

Below MIC concentrations of PSo-4 and Ooc-1 were used for AFM (75 to 100 µM and 100 to 200 µM respectively) so as to allow for analysis of partially affected cell membranes.

AFM measured height (Figure 13A) and amplitude (Figure 13B) images highlight the differences between the untreated control and *E. coli* cells exposed to PSo-4 and Ooc-1. It is clear that both peptides have a devastating effect on the cell membrane, even at lower concentrations than the MIC, with PSo-4 seemingly promoting a complete disintegration of the cell while Ooc-1 images give the impression that the peptide is accumulating on and around the cell membrane making one of its ends look engorged. This can be observed in the measured height image for Ooc-1 too as we can see that the height for the affected cell end is much increased in comparison to the rest of the cell.

The increased values of *E. coli*'s surface roughness and height measurements for Ooc-1 (Figure 14 B1 – B2) support the idea that this peptide appears to be gathering on the membrane surface of cells in a concentration-dependent manner, covering it and causing its disruption, possibly in the style of the carpet model. However, the same is not the case for PSo-4 (Figure 14 A1 – A2) considering its surface roughness and height assessments demonstrate that no significant change was observed. We can hypothesise that maybe PSo-4 does not act on Gram-negative bacteria like *E. coli* by flooding its membrane surface, but instead it might be very successful at quickly interfering with a metabolic pathway or at triggering a signal for cell apoptosis.

A

B

Control

100 μM PSo-4
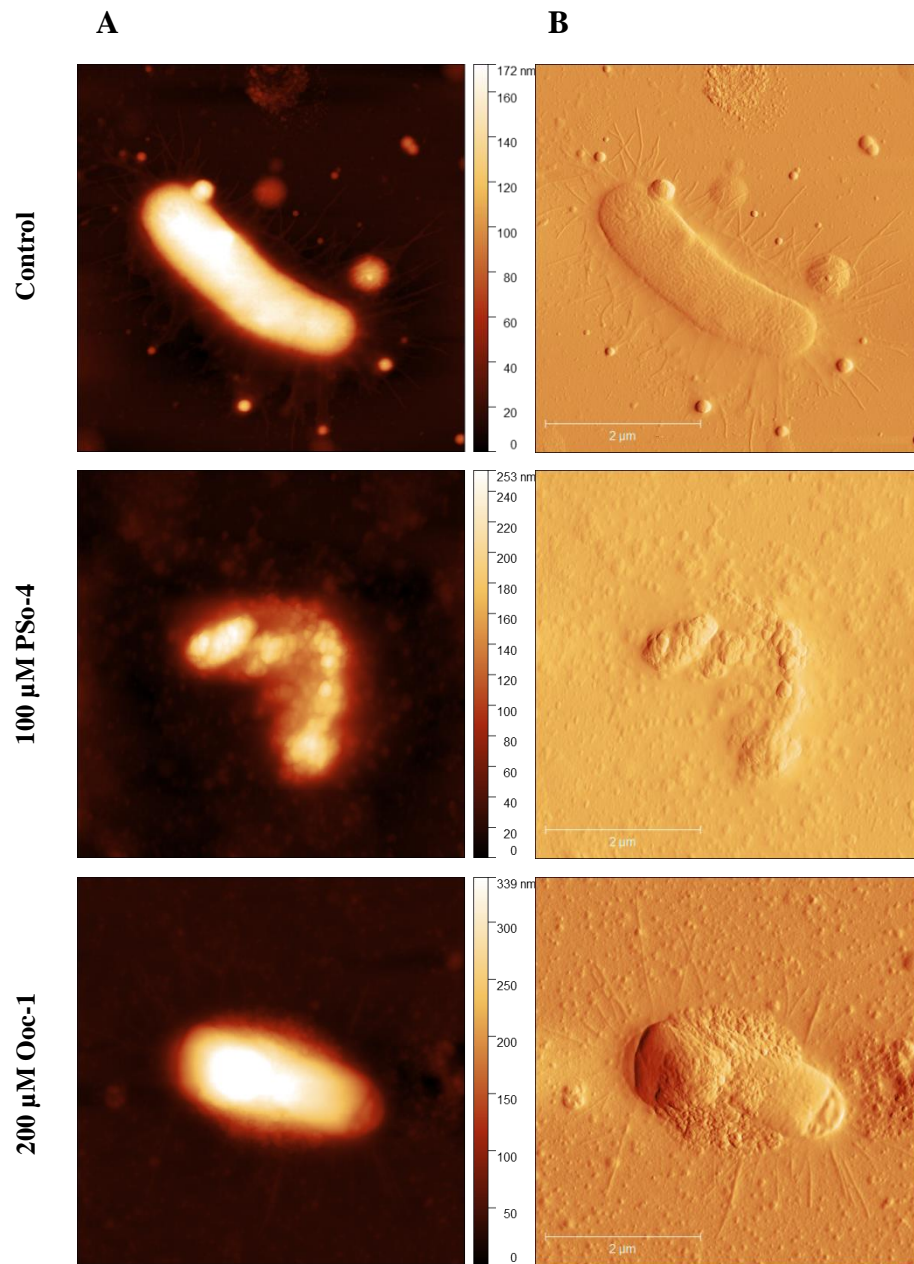
200 μM Ooc-1

Figure 13. AFM height (A) and amplitude (B) images of *E. coli* ATCC 25922 after exposure to 100 μM of PSo-4 and 200 μM of Ooc-1. Control images represent untreated cells. These images were acquired with the help of Marco M. Domingues, PhD, and PhD student Constança P. Amaral from Nuno Santos Lab – iMM.
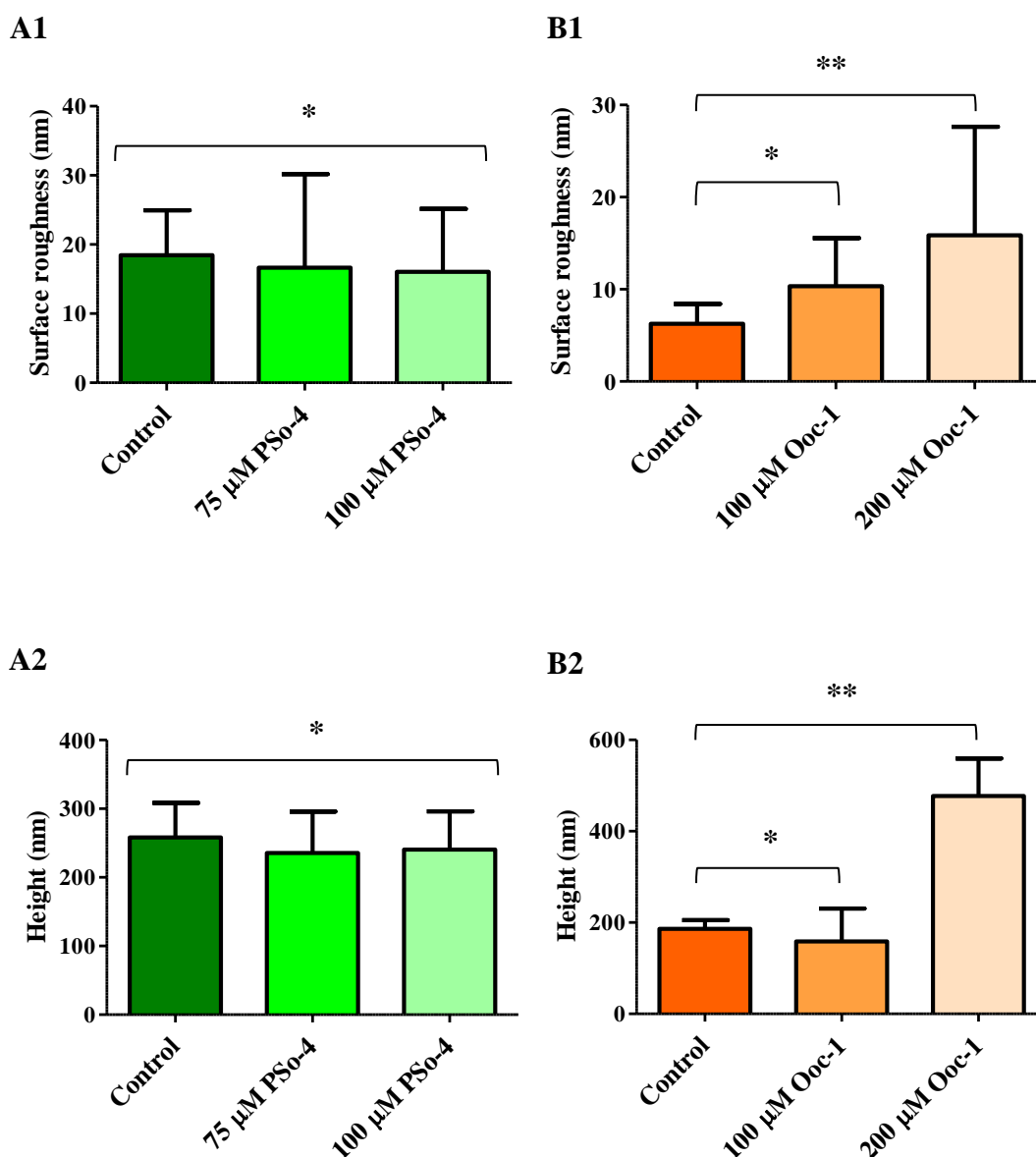
Figure 14. Measurement of variation in *E. coli*'s surface roughness (A1 – B1) and cell height (A2 – B2) when exposed to different concentrations of PSo-4 and Ooc-1. Control columns characterise untreated cells; Error bars represent mean (SD). * signifies $p > 0.05$ for comparison between treated samples and untreated control; ** represents $p < 0.05$ for comparison between treated samples and untreated control.

3.3 Ooc-1 hints at a deleterious effect on *T. b. brucei* 427 wt

As there are no replicates for this experiment, we can only speculate in relation to the results obtained. Nevertheless, if future assays corroborate these results then it would be of high value to further investigate the action of the peptide Ooc-1 on *T. b. brucei* since it was the only peptide that caused a strong reduction in the parasite's viability to only 5% at the concentration of 100 µM (Figure 15) after 72 h incubation period. This was

also visually confirmed under the light microscope, where it was clear that the number of parasites in the wells containing 100 µM of Ooc-1 was much reduced in comparison to the wells holding the remaining Ooc-1 concentrations and the control (-) wells.
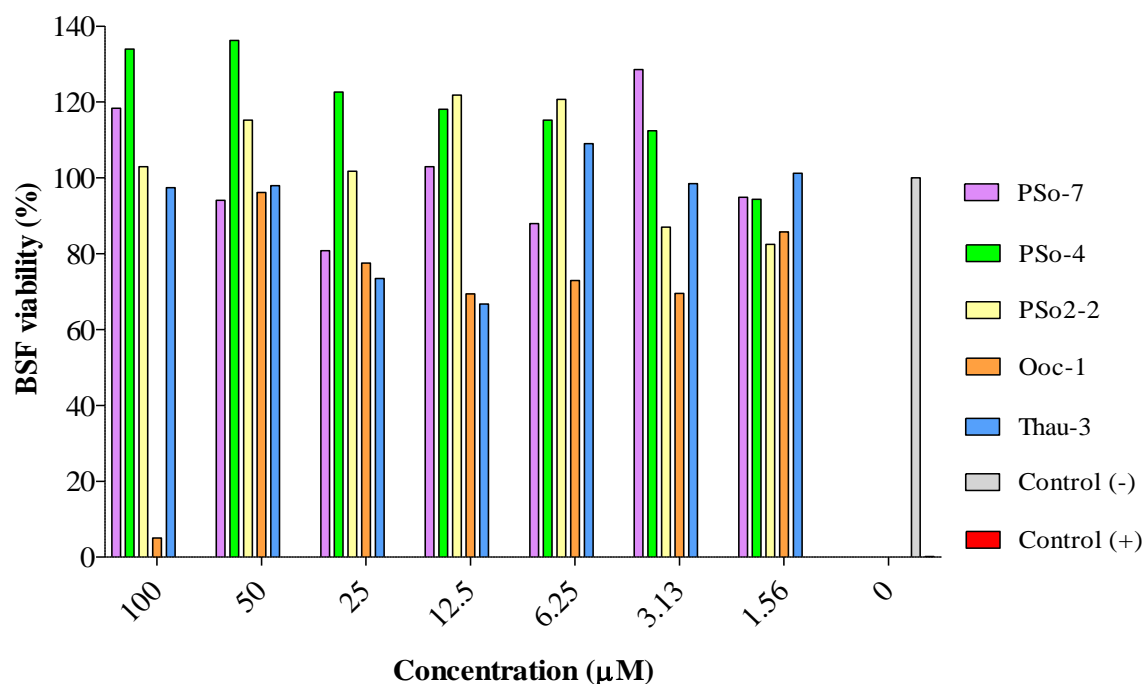

Figure 15. Viability of bloodstream forms of *T. b. brucei* Lister 427 wt after 72 hours incubation with Patagonian amphibians' derived peptides. Control (-) = Untreated BSFs; Control (+) = 10% Triton X-100 treated BSFs. $p < 0.05$ for comparisons between treated cells and control (-) was only observed for control (+) and Ooc-1 at the concentration of 100 µM. Control (+) y axis values are < 0%.

All other peptides had no significant effect on the parasite, in fact it can be observed that the BSF viability response doesn't seem to correlate with the concentration of the peptides and that there are cases where BSF viability is higher than 100%. This may imply that what we are actually seeing is an overexpression of metabolic response by *T. b. brucei* BSFs to the presence of our peptides since alamarBlue permeates the cell membrane and is reduced in the cytoplasm to its fluorescent form by mitochondrial-reductases, cytochromes and other enzymes present. It could also be the case that further optimisation of the assay conditions is necessary or simply that it was an operator's error and thus, as mentioned previously, it would be of value to replicate this assay a few more times.

3.4 Huh-7 cells seem to be susceptible to the action of most tested peptides

Most of our peptides were quite successful in decreasing Huh-7 cells viability. PSo-7 and PSo-4 showed a promising reduction of Huh-7 viability to below 25% at concentrations of only 1 µM, although PSo-4 reveals a statistically non-significant result at 10 µM (Figure 16), while PSo2-2 at 42 µM was able to reduce cell viability to 0% (Figure 17).

Peptide Thau-3 managed to imprint a relatively constant level of cell viability shrinkage below 40%, being able to bring it down further to < 30% at 250 µM concentration. However, statistical analysis for Thau-3 results when compared to the results for untreated cell revealed a $p > 0.05$ deeming Thau-3 action on Huh-7 cells statistically irrelevant (Figure 16). Nevertheless, we believe Thau-3 remains a good candidate for further anticancer studies.
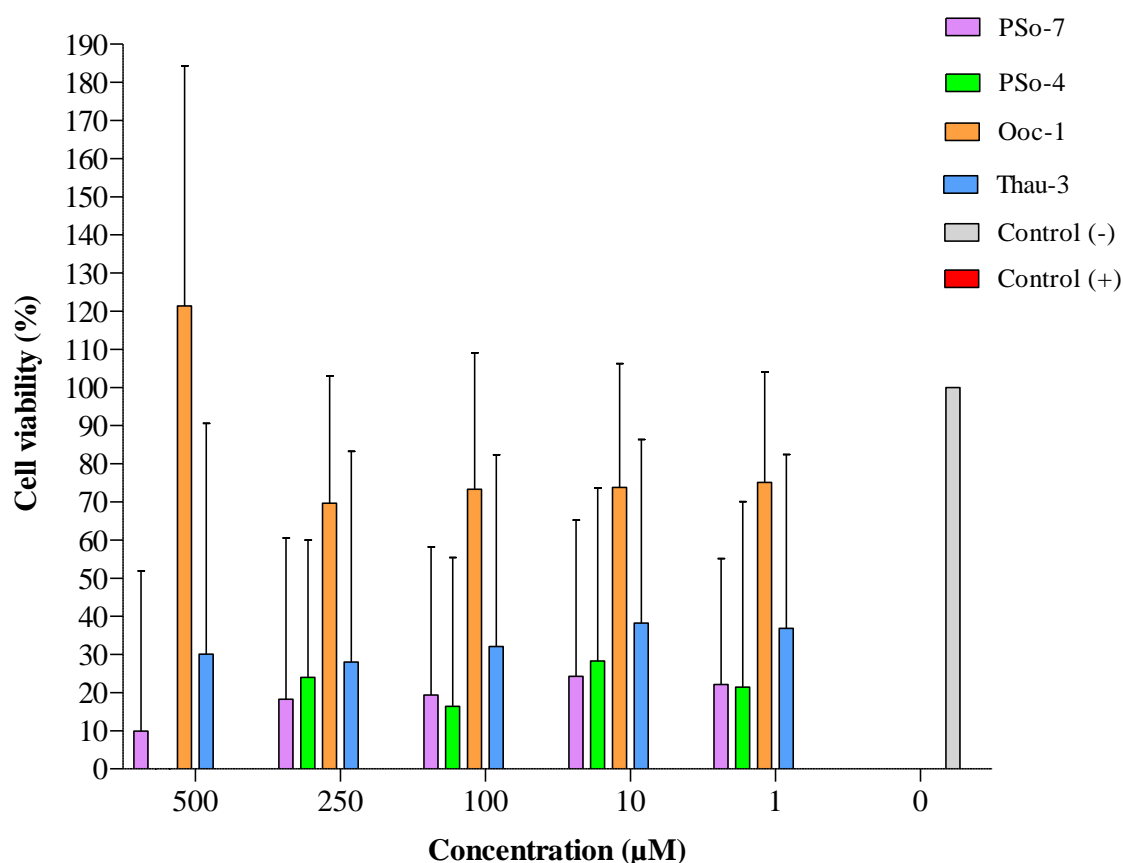
Figure 16. Viability of Huh-7 after 24 hours exposure to Patagonian amphibians' derived peptides. Control (-) = Untreated cells; control (+) = 10% Triton X-100 treated cells. $p < 0.05$, for comparisons between treated cells and control (-), was observed for all concentrations of PSo-7 and for PSo-4 at concentrations of 500, 250, 100, 1 µM. $p > 0.05$, for comparisons between treated cells and control (-), was observed for all concentrations of Thau-3, Ooc-1 and PSo-4 at the concentration of 10 µM. Control (+) y axis values are < 0%. Error bars represent the mean (SD).
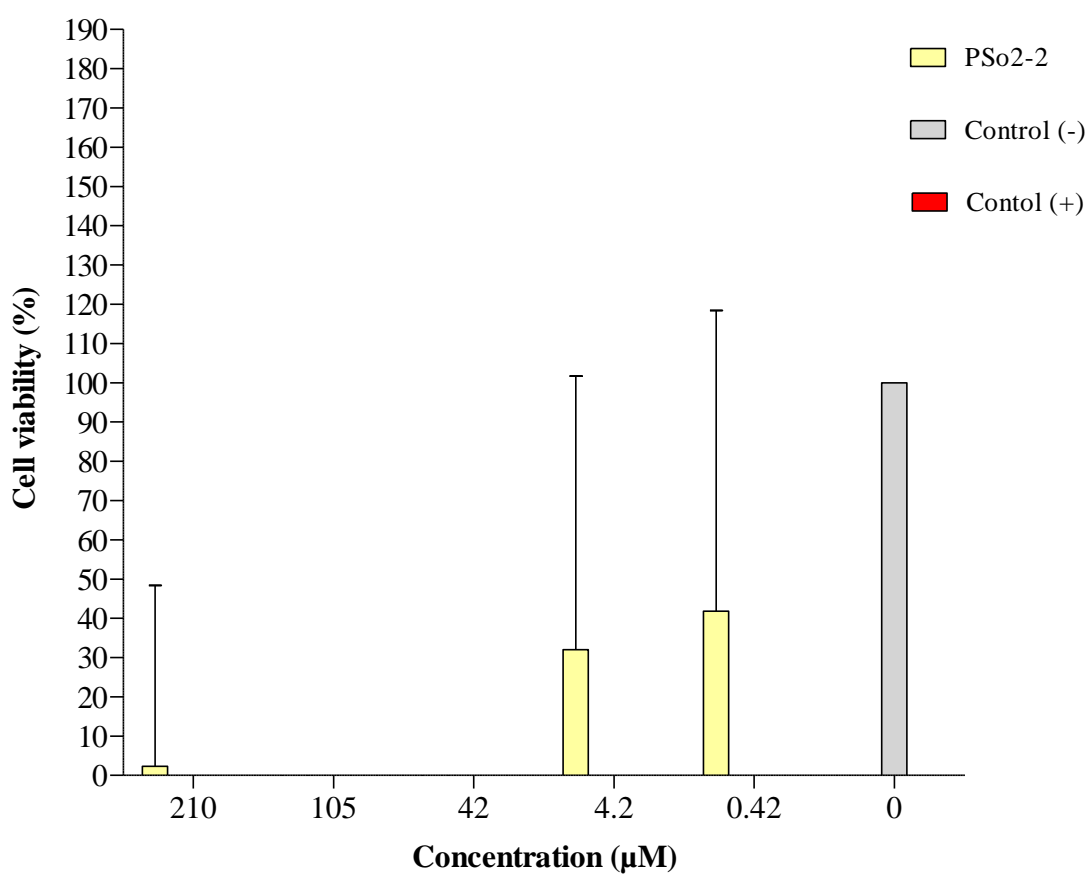
Figure 17. Viability of Huh-7 after 24 hours exposure to Patagonian amphibians' derived peptide PSo2-2. PSo2-2 tested concentrations differ from the remaining peptides due to an initial error with PSo2-2 stock concentration. Control (-) = Untreated cells; control (+) = 10% Triton X-100 treated cells. $p < 0.05$, for comparisons between treated cells and control (-), was observed for PSo2-2 at concentrations of 210, 105 and 42µM. $p > 0.05$, for comparisons between treated cells and control (-), was observed for PSo2-2 concentrations of 4.2 and 0.42 µM. Control (+) y axis values are $< 0\%$. Error bars represent the mean (SD).

Ooc-1 produced the poorest of outcomes amongst all the peptides tested, not being able to decrease cell viability much below the 70% mark (Figure 16) which is interesting considering that Ooc-1 was the peptide that showed the highest capability to cause apoptosis and necrosis ($\approx$ 9 % and 10 % respectively) on healthy cells (Appendix 10).

These results however show high SD values for all peptides tested, meaning there is a high variability between the means of the replicates. We believe that this might be due to the fact that the XTT assay is based on absorbance and the peptides might be causing an extra background effect. As such, further optimisation of this assay would probably be necessary to confirm peptide action.

3.5 ANS fluorescence measurements show the degree of peptide aggregation in PBS solution

Peptides showed some degree of aggregation when in PBS solution (Figure 18 A1 – A5). This occurrence also proved to be concentration-dependent for all peptides with an increase in fluorescence intensity and in blue shift of the spectra alongside the rise in peptide concentration. Peptide concentrations used for ANS titration were individually adjusted, per peptide, based on each spectrum response. This was due to peptides stock low availability.

PSo-7 and PSo-4 peptides displayed the lowest amount of aggregation when compared to the other peptides in the test group. PSo-7 only showed a more significant, but still small, blue shift (0.3%) and increase in fluorescence emission ($\approx$ 11%) at the concentration of 500 µM (Figure 18 A1) while PSo-4 exhibited a similar behaviour at lower concentrations of 200 – 350 µM (Figure 18 A2). Occupying the middle ground we find Thau-3, expressing ever so slightly higher levels of aggregation than PSo-4, at concentrations of 150 µM. It then takes off with a more aggressive shift at 300 – 500 µM (Figure 18 A3).

PSo2-2 proved to possess a higher tendency for aggregation even at smaller concentration like 20 µM. At 100 µM, the highest concentration tested for this peptide, PSo2-2 demonstrates an increase in fluorescence intensity > 50% when compared to the reference sample (0 µM PSo2-2) and there was also a blue shift of $\approx$ 7% (Figure 18 A4)

Peptide Ooc-1 tops the list in this aggregation chart. The spectrum for Ooc-1 shows an increase of more than 10-fold in intensity when compared to the reference sample and most of the other peptides at 100 µM (Figure 18 A5). The blue shift onto the higher energy side of the spectrum is quite obvious and pronounced in this peptide's case.

Plotted results for all peptides in relation to F_{Imax} and λ_{max} (Figure 19 A1 and Figure 19 A2) give a clearer general picture as to the differences occurring in F_I increase and blue shift between the peptides tested.

Figure 18. Peptides aggregation spectra with ANS dye. The probe ANS was titrated with peptides
PSo-7 (A1), PSo-4 (A2), Thau-3 (A3), PSo2-2 (A4) and Ooc-1 (A5) until significant changes were
seen in the spectra. The fluorescence intensity was normalised to the summation of the ANS intensity
in the reference samples which contained zero addition of peptides. Each spectrum is representative
of their respective replicates illustrated in the Appendix section.

A1
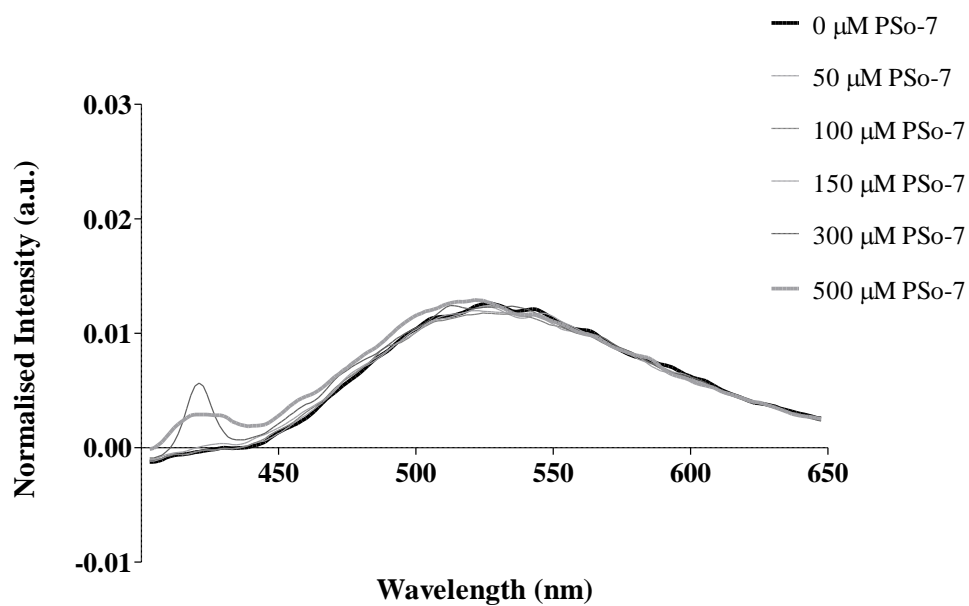
A2
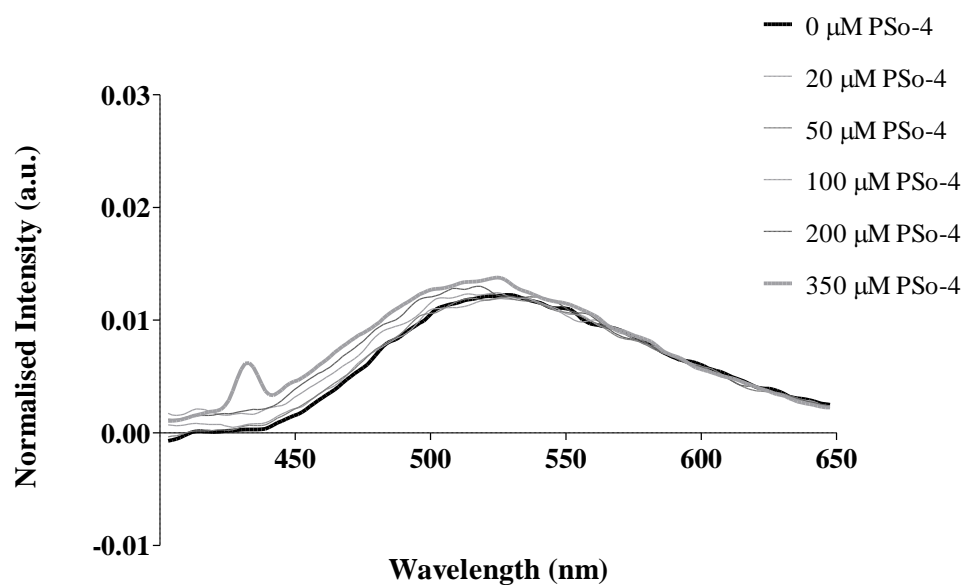
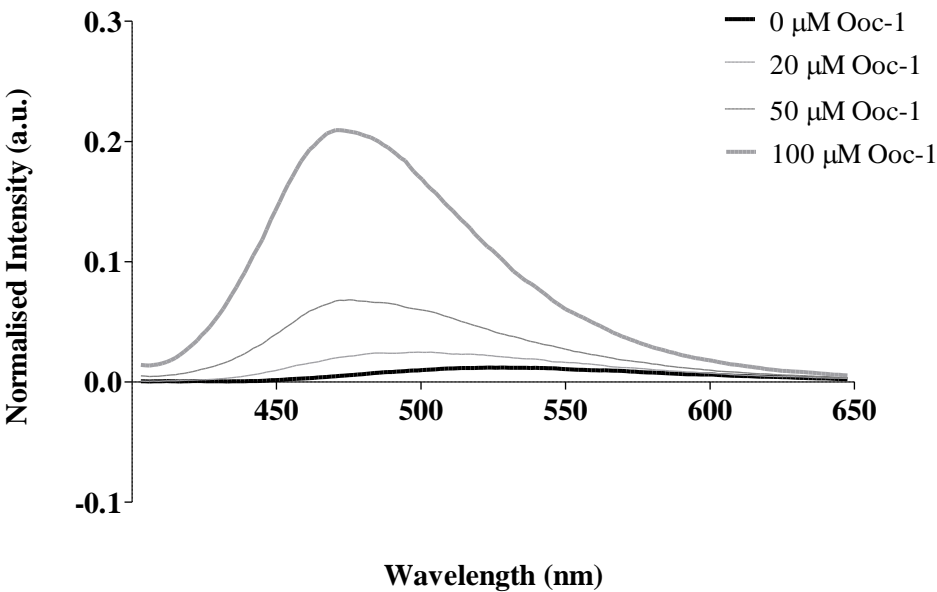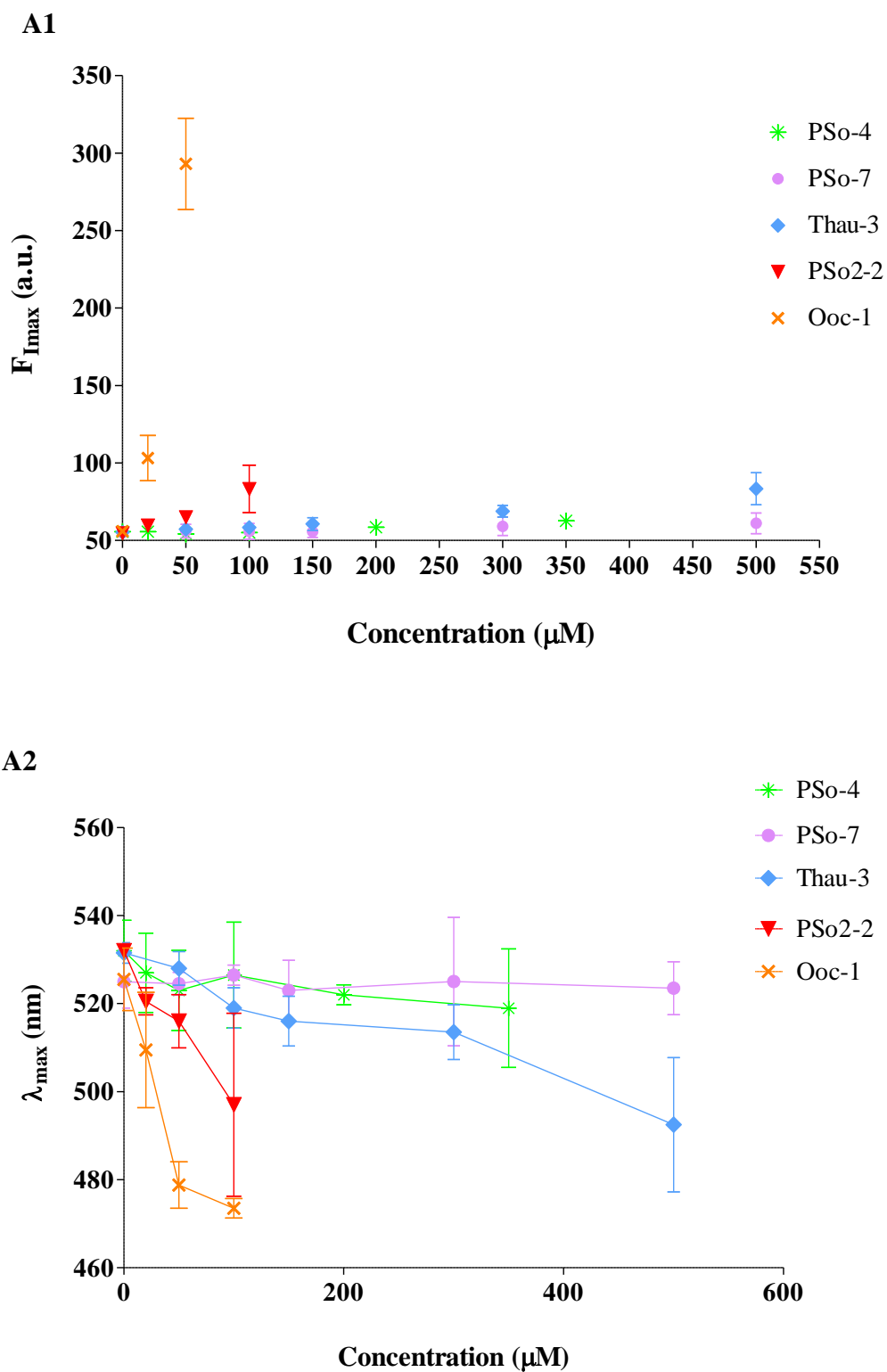**A3**
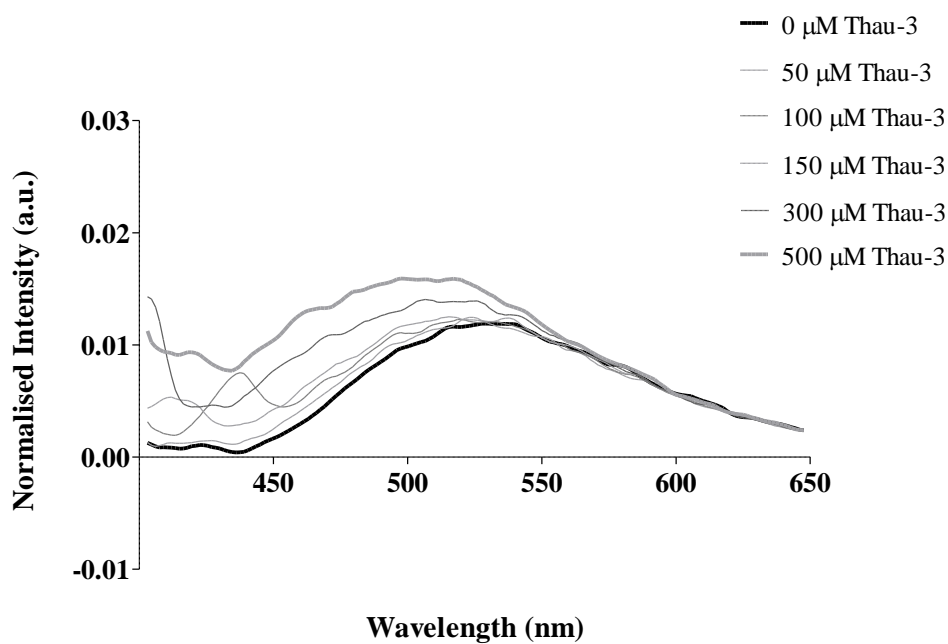
A4
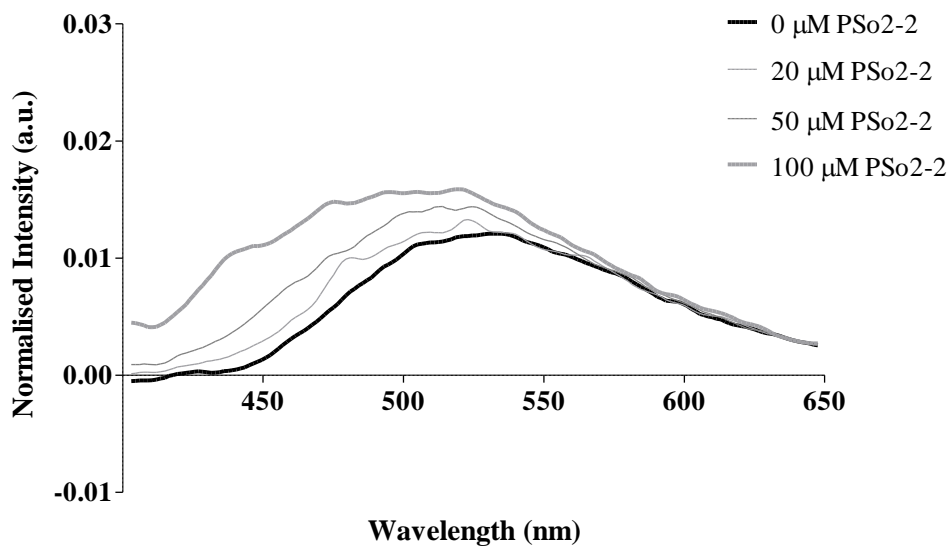
A5

Figure 19. Peptides aggregation response with ANS dye. Representation of the response of F_{Imax} (A1) and of λ_{max} (A2) to the increasing concentrations of each peptide. Error bars signify mean (SD).

3.6 CD studies hint at peptides' secondary structures in POPC:POPG lipid solution

Preliminary CD studies revealed some interesting behaviour from our peptides when in contact with POPC:POPG (1:1) LUVs. As mentioned previously, POPC:POPG LUVs model was chosen because it mimics, to a certain extent, the anionic membranes of bacteria and cancer cells. Even though LUVs can cause light scattering effects, that may lead to spectra distortion due to their larger size when compared with small unilamellar vesicles, their use is not without advantages. LUVs are easy to prepare, stable for several days at room temperature, are able of encompassing a double bilayer and have a smaller membrane curvature making them a good model for biological membranes and to study their interaction with HDPs.

CD results showed that peptides PSo-7 and PSo-4 in PBS (Figure 20 A1 and Figure 20 B1) retained a random coil conformation with noticeable negative bands nearby 200 nm and weak positives near 220-230 nm which are characteristic of this type of conformation as described elsewhere [56]. Upon contact with the LUVs, the spectrum for PSo-7 did not alter (Figure 20 A2) apart from an upsurge in noise due to an increase in scattering from the LUV surface, meaning that this peptide's secondary structure remained a random coil. In the spectrum of PSo-4 in solution with LUVs is possible to see the existence of some noise (Figure 20 B2) between 200 – 215 nm, however, this seems to be the same sort of occurrence described above for PSo-7. As the ratio between the concentration of lipid/peptide increases, and overall peptide concentration in solution decreases to 179 µM, a shift occurs but overall PSo-4 maintains a random coil conformation. There is the possibility of an isodichroic point around 213 nm but it is not clear, nevertheless, if there was an isodichroic point it could be argued that PSo-4 is transitioning from one random coil conformation to another and thus having two different peptide structural species in solution. Overall, PSo-4 spectrum does not hint at a transition to a more ordered conformational state.

Thau-3 reveals a striking shift from a random coil in aqueous solution (Figure 20 C1) to a more ordered but still irregular structure, in the presence of POPC:POPG (Figure 20 C2), that possibly contains α-helix, random coil and β-sheet portions, as illustrated by its isodichroic point so close to 200 nm and by the fact that its spectrum is very similar to the one for the small protein aprotinin [70,71]. Fourier-transform infrared spectroscopy

(FTIR) analysis would have to be performed in order to undoubtedly confirm the presence of a β-sheet portion in this peptide.

The representative spectrum for PSo2-2 in aqueous solution (Figure 20 D1) presents a mix of random coil plus α-helix, with distinctive double negative minima at ~ 205 and 222 nm. Addition of lipid originates transition to a more structured conformation of α-helix content (Figure 20 D2). It appears to be a simple mechanism governed by a simple event (less folded to more folded → less random to more α-helix signal). The existence of an isodichroic point at 205 nm indicates this simple mechanism of two conformations [70].

Ooc-1 secondary structure spectrum in PBS (Figure 20 E1) is very similar to that already described for PSo2-2. With addition of lipid, its arrangement gains more α-helix (Figure 20 E2) but there seems to be a loss of signal in the middle additions, between the concentrations of 200 and 191 µM of peptide, followed by a signal recovery. It is possible that this event occurred due to an initial aggregation in solution which is then reverted by the further additions of lipid and the additional gain of α-helix.

Figure 20. CD spectra of Patagonian amphibians' derived peptides. Peptides PSo-7 (A1 – A2), PSo-4 (B1 – B2), Thau-3 (C1 – C2), PSo2-2 (D1 – D2) and Ooc-1 (E1 – E2) spectra of secondary structures when in PBS (column 1) and titrated with POPG:POPC LUVs (column 2). Increasing lipid concentrations in the cuvette equal a decrease in peptide concentration.
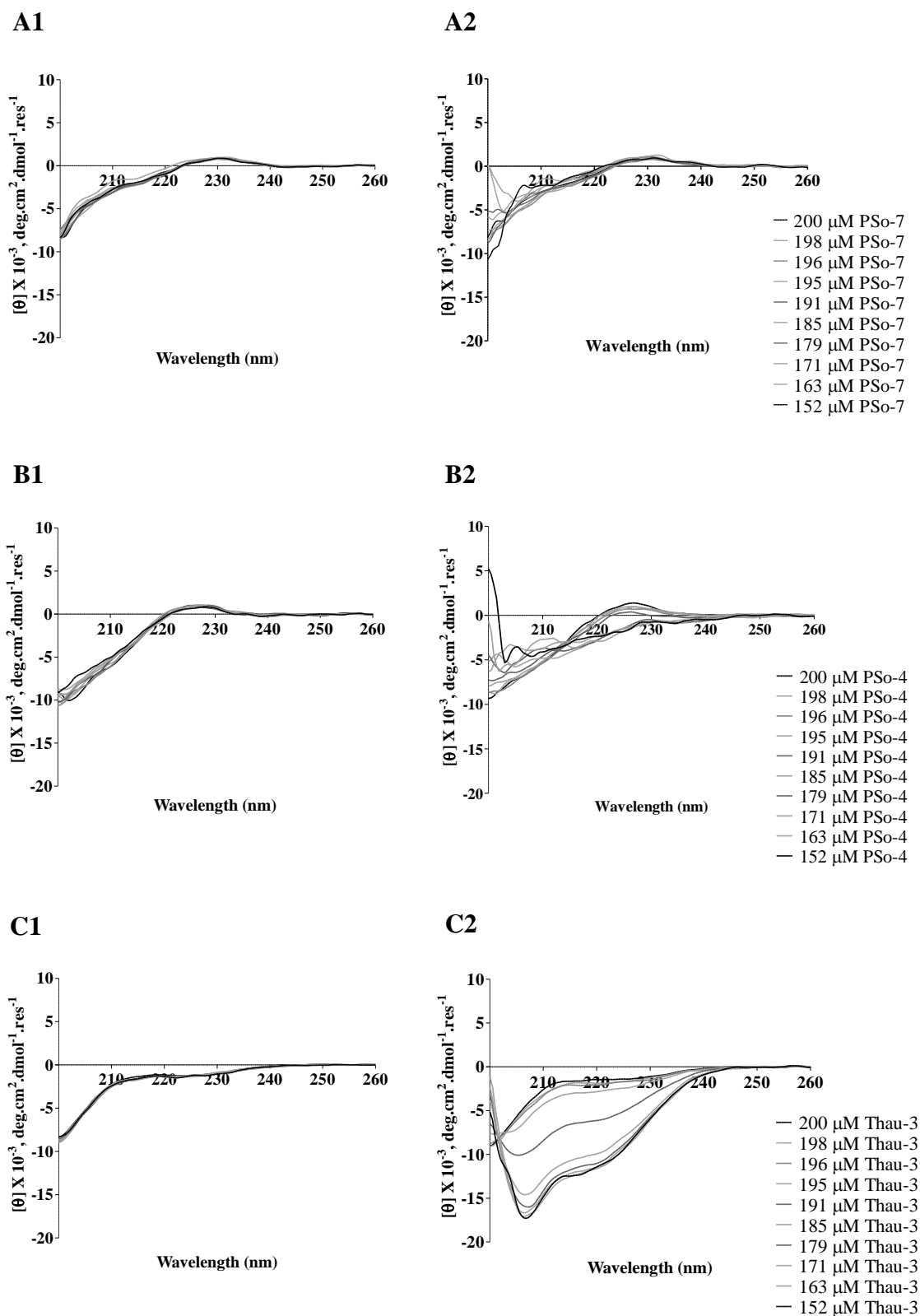
D1
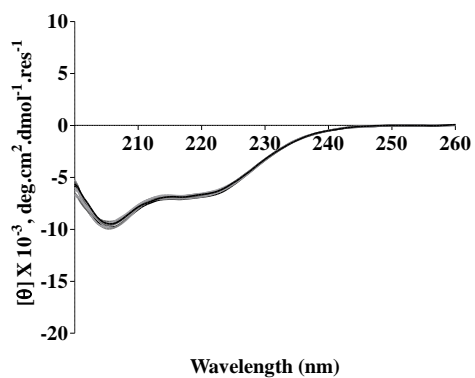
D2
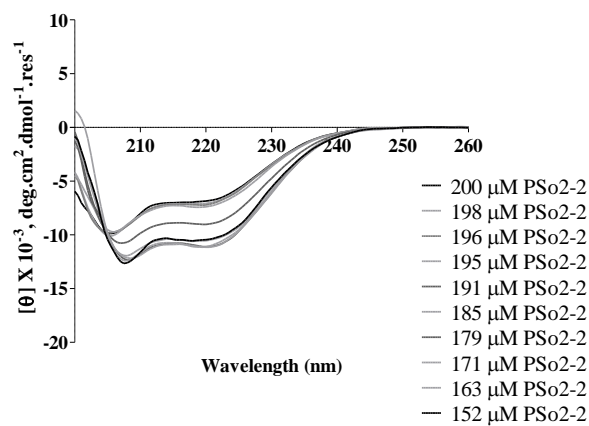
E1
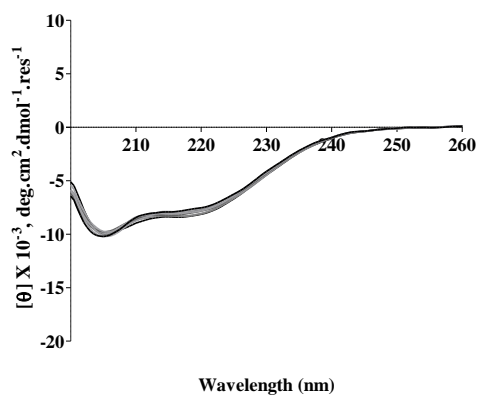
E2
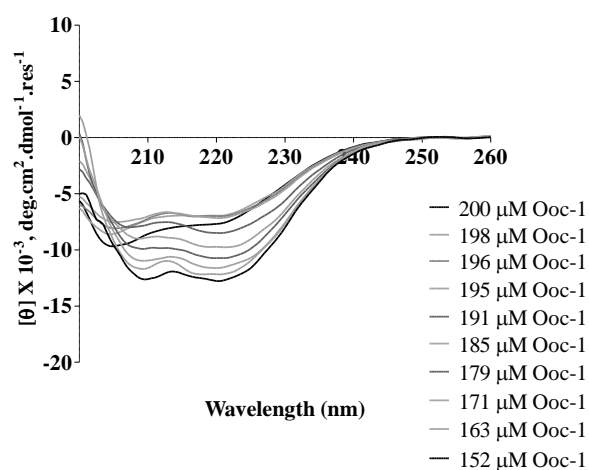
4 Discussion and Conclusions

The mode of action of AMPs on bacteria cell walls rests on the structural and physical interactions of the AMP with the anionic bacterial membrane; as mentioned before, bacteria commonly fall into two groups: Gram-negative or Gram-positive, depending on the structure of their cell envelopes. The differences lay heavily on their outer cell envelope with Gram-positive bacteria having a thick matrix formed by a layer of crosslinked peptidoglycan with nano-sized pores and dotted with negatively charged teichoic acid which surrounds the cytoplasmic membrane [72]. Contrastingly, Gram-negative bacteria own a much thinner and less cross-linked peptidoglycan layer which is placed between a lipopolysaccharide (LPS) rich outer membrane and an inner membrane consisting purely of zwitterionic and anionic phospholipids [72].

Effective AMPs against Gram-negative bacteria need to be able to disrupt both outer and inner membranes of the cell envelop to be successful. This may prove more difficult than it sounds since even though LPS molecules on the outer membrane have a high number of negatively charged phosphate groups, which would be expected to attract AMPs, they also interact with divalent cations such as Ca^{2+} and Mg^{2+} forming salt-bridges. This creates a sort of electrostatic region that can serve as a barrier to hydrophobic molecules [72].

Disruption of Gram-positive bacteria cell wall by AMPs would, in theory, be easier than that of Gram-negative, and yet, it isn't that straightforward. The existence of the already mentioned nano-sized pores in the peptidoglycan of Gram-positive bacteria may facilitate the diffusion of AMPs and their accumulation on the surface of the inner membrane [72,73]. However, this may be highly dependent on the successful interactions between AMPs and teichoic acid polymers - wall teichoic acid (WTA) and cytoplasmic membrane lipoteichoic acid (LTA); as previously reported for other AMPs like mellitin and cecropin [74].

Another factor that might contribute towards the success or failure of AMPs against Gram-negative and Gram-positive bacteria is the variation in composition of the inner membrane phospholipid bilayer as well as its headgroups and fatty acid moieties [73]. Gram-positive bacteria inner membranes are characterized by having large portions of negatively charged phosphatidylglycerol (PG) while Gram-negative bacteria present

larger fractions of the zwitterionic phosphatidylethanolamine (PE) and PG [73].

Contrasting with bacterial cell membranes, *T. brucei brucei* bloodstream form parasites possess a cell membrane that resembles that of eukaryotic cells with the most abundant classes of phospholipids present being phosphatidylcholine (PC) and PE [75]. Furthermore, BSF membranes are known for being fluid and dynamic to accommodate the levels of motility, endocytosis, vesicle trafficking and lateral flow of surface molecules required by these organisms [76]. The surface of BSF membranes is also densely coated by a variant-surface glycoprotein (VSG) which provides the means of escape from the host's immune system by antigenic variation [77].

So, for an AMP to be able to interact with *T. b. brucei* BSFs and exert trypanocidal activity, it would have to bypass the steric hindrance produced by the high density of VSG on the BSF cell membranes in order to interact with the plasma membrane while showing affinity for the phospholipid groups present [76].

For cancer cells, the characteristic negative charge of their cell membranes that allow anticancer peptides to interact comes as a result of an increased expression and membrane reshuffling of anionic molecules such as PS, O-glycosylated mucins, sialilated gangliosides and heparan sulphates [78], setting them apart from normal healthy mammalian cells.

The results in relation to the peptides studied in this project demonstrate that they have the potential of exerting deleterious action over at least one of the target cells investigated (Table 6).

	Antibacterial activity				Antiparasitic activity	Anticancer activity
	E. coli MIC		*S. aureus* MIC		*T. b. brucei*	Huh-7 cells
	μM	μg/ml	μM	μg/ml	μM	μM
Thau-3	457 *	600 *	> 381 *	> 500 *	> 100	> 500
PSo2-2	> 250 *	> 700 *	> 250 *	> 700 *	> 100	0.42
PSo-7	474 *	700 *	> 474 *	> 700 *	> 100	1
PSo-4	180 *	250 *	> 360 *	> 500 *	> 100	1
Ooc-1	500	1073	> 500	> 1073	100	> 500

Table 6. Summary of the antibacterial, antiparasitic and anticancer properties of the peptides tested. Apart from Thau-3 [33], data on the remaining peptides of this test group has never been published. * denotes the peptides whose MICs were performed by Lorena Cancelarich, PhD student, from Mariela M. Marani's lab at IPEEC-CONICET.

Even though the data obtained does not allow for a concrete inference of how exactly these peptides are interacting with their targets, we can hypothesise as to the mode of action and target affinity of PSo-7, PSo-4, Thau-3, PSo2-2 and Ooc-1 and how their activity might be directed and modulated by the amino acid residues present in their sequence, surface charge, stability and conformational changes in solution.

Peptide Thau-3 is leucine (L) (30%), G (23%) and K (15%) rich. Both L and G are hydrophobic amino acid residues while K is basic and positively charged. Thau-3 has a + 2 net charge and an alkaline pI of 10. Looking at the sequence of this peptide we can see that, theoretically, four hydrophobic amino acid residues exist on the same surface and could interact with membrane lipids. Although, this number might not be completely accurate considering the CD results that point towards Thau-3 changing from a random coil structure into an irregular secondary structure (α-helix / random coil / possibly β-sheet) instead of a more ordered structure when in contact with POPC:POPG LUVs. The last two residues on the C-terminal of Thau-3 are both K which, as previously mentioned, is a basic, positively charged amino acid with side chains that often forms salt bridges. On the N-terminal we find the polar asparagine (N) occupying the first position. This amino acid contains an amide group that often acts as a proton donor or acceptor, forming hydrogen bonds. Another characteristic showed by Thau-3 was a tendency for moderate self-aggregation.

PSo2-2 peptide expressed a secondary structure with random coil plus α-helix content in aqueous solution and we saw that the α-helix signal increased with further additions of POPC:POPG hinting that this peptide does interact with this membrane model. In addition, this peptide also showed a high propensity to self-aggregate. With a net charge of + 2 and pI of 9.69, structurally, this peptide is rich in R (21%), alanine (A) (17%), L (17%) and tyrosine (Y) (13%). Apart from the basic and positively charged R, the remaining high content residues are either hydrophobic (A and L) or amphipathic (Y) and are found mainly concentrated in proximity of the C-terminal with seven estimated hydrophobic amino acids on the same surface. On the N-terminal, positions 1, 2 and 3 are occupied by two Y and a polar glutamine (Q). Both Y and Q act as proton donor/acceptor due to the presence of a − OH and amide group respectively, thus, are able to form hydrogen bonds.

The peptides PSo-7 and PSo-4 were the only ones that showed very little

predisposition for self-aggregation as well as not producing a helix or sheet secondary structure. Instead both peptides adhered to a random coil structure in aqueous solution. PSo-7 didn't show any changes when in contact with POPC:POPG LUVs while PSo-4 displayed a shift into a second structural specie of random coil. Both peptides present with a theoretical alkaline pI of 9.53 and 11 respectively. They share similar sequence length, net charge (+ 2 for PSo-7 and +3 for PSo-4) and N-terminal residues in the 1st and 2nd positions – phenylalanine (F) and I. However, the similarities stop there since PSo-4 is a R (20%) and I (20%) rich peptide while PSo-7 is 27% Y. All hydrophobic residues of PSo-4 are concentrated in the first six positions of its sequence, (two of them predicted to share the same surface) followed by strong cationic C-terminal with R and K residues, whereas PSo-7 has hydrophobic amino acids in the first three positions of its sequence (none predicted on the same surface) but its C-terminal is composed of two amphipathic Y amino acids.

The only neutrally charged peptide of this test group, Ooc-1, is also singular in its ever so slightly acidic pI of 6.75. In matters of amino acid content it shows an abundance of hydrophobic residues with 21% of L and 15% of valine (V), plus 10% of the basic R, and polar amino acids in the form of asparagine (N) (15%) and threonine (T) (10%). Its N-terminal is polar with N in the 1st position able to from hydrogen bonds through its amide group. The C-terminal is positively charged with R followed by the presence of the polar T. Ooc-1 also showed interaction with POPC:POPG LUVs by acquiring a secondary conformation of random coil with increasing α-helix, meaning that it is capable of interacting with these membranes, but it was also the peptide that showed the highest rates of self-aggregation when in aqueous solution.

Looking at the results obtained for the antibacterial capacity of our peptides (Table 6) it is clear that, in the concentrations tested, none show activity against the Gram-positive *S. aureus* while most show relatively weak antimicrobial activity against *E. coli* when compared to other peptides described in literature (Table 7). PSo-4 displayed the highest antimicrobial action of the test group while PSo2-2 did not exhibit any deleterious effect, although, there should be noted that the highest concentration tested for this peptide wasn't as high as the concentrations for some of the other peptides.

The lack of activity of our peptides against *S. aureus* can be due to a multitude of physicochemical factors. There might be an inability to cross the peptidoglycan wall of

S. aureus due to peptide self-aggregation or a lack of affinity or productive electrostatic interactions with its cell wall components like LTA [73]. Further studies relating to membrane interactions with different lipids and lipid contents to mimic Gram-positive cell membranes are necessary in order for a clearer assessment.

In relation to the activity showed against Gram-negative *E. coli*, it might be possible that the net charge of each peptide plays a big role here as all tested peptides with a net charge below + 3 showed little to no activity while PSo-4 (net charge + 3) showed higher potency. The seemingly importance of a positive charge threshold for antimicrobial activity has also been previously reported for several peptides including those of the magainin family [79] and more recently in the study that identified Thaulin-1 (Table 7) and Thau-3 [33]. Another important factor in the antimicrobial activity of the tested peptides appears to be the residues present at the C-terminal of these compounds. As mentioned previously, there are certain residues, like K and R, that are known to be advantageous for AMPs properties when occupying positions at the C-terminal since it is this terminus that first interacts with the bacterial cell membrane and penetrates it [34]. When looking at the sequence of our peptides, we can see that most of them possess at least one of these amino acids at the end of their sequence but it is PSo-4 that truly showcases a strong cationic C-terminal with both K and R present. These residues are capable of forming ionic interactions, hydrogen bonds and to interact with water molecules, furthermore, R is able to interact in three different directions due to its guanidinium group which possess three asymmetrical nitrogen atoms [80]. PSo-4 is then possibly able to form a large number of electrostatic interactions, such as salt-bridges, and to compete with divalent cations Ca^{2+} / Mg^{2+} for binding with LPS molecules on Gram-negative cell wall. This allows it to adsorb onto the cell membrane where its hydrophobic moieties could interact with phosphate groups or LPS lipid tails and destabilise the outer membrane packing, leading to its permeabilization and/or disruption in order to reach the bacteria's cytoplasmic membrane. Outer membrane permeabilization of Gram-negative bacteria through interaction with LPS has been previously reported for AMPs such as defensins and magainins [81]. Such mechanism would be in line with the complete obliteration of *E. coli* cells by PSo-4, even at concentrations below the MIC, and the lack of an increase in cell surface roughness as shown by AFM images and analysis, whereas for Ooc-1 AFM data seems to suggest a

concentration dependant action that may fall within the membranolytic carpet model. Trypanocidal activity was only displayed by Ooc-1, which at the concentration of 100 µM managed to reduce the viability of BSFs to < 5% after 72 h incubation period. Even though this is only a preliminary result, we can speculate that Ooc-1 might be able to circumvent the steric hindrance from VSG and interact with the plasma membrane of *T b. brucei* BSFs. Several cationic AMPs are known to possess trypanocidal capability over *T. brucei* BSFs (attacin, stomoxyn, pleurocidin, indolicin and some human antimicrobial compounds like the neuropeptide VIP), but few neutrally charged AMPs have been described [82,83]. SHP-1, a neutrally charged peptide, derived from the N-terminal signal of the human haptoglobin-related protein, capable of killing BSFs of *T. b. brucei* 427 (Table 7), shows some similarities with Ooc-1 in matters of net charge, high core hydrophobic content and even in secondary structure (random coil with α-helix content) [76,83]. Therefore, Ooc-1 action over *T. b. brucei* BSFs might be similar to SHP-1whose hydrophobic core region, made up of 10 amino acids, has proven to be crucial for BSF killing by specifically targeting fluid membranes and decreasing or distorting their physical properties and/or stability by permeabilization [76]. Furthermore, Ooc-1 demonstrated the highest cytotoxicity values of this test group against healthy mouse macrophage cells (Appendix 10), which reveals this peptide's capability for interacting with the zwitterionic phospholipid PC that is also abundant in BSF cell membranes [75].

Further testing, including membrane models − peptide interaction studies, alongside flow cytometry and liposomes leakage assays, would be invaluable to confirm Ooc-1 true mode of action.

HCC Huh-7 cells showed relevant susceptibility to PSo2-2 (42 µM), PSo-4 (1 µM) and PSo-7 (1 µM) (Table 6). Thau-3 was able to imprint some reduction in Huh-7 cells viability but, statistically, this reduction was considered insignificant. Nevertheless, it should be noted that Thau-3 sequence shows ≈ 53% homology with Frenatins 2.1S, 2.2S and 2.3S. These peptides share the same or similar net charge with Thau-3 (+1 and + 2 respectively) as well as many hydrophobic core residues and have originated from the skin secretions of the South American Orinoco lime tree frog [84]. Frenatins 2.1S, 2.2S have shown a stronger anticancer activity than frenatin 2.3S; this has been linked to the higher net charge and more stable α-helix secondary structure of frenatins 2.1S and

2.2S, whereas frenatin 2.3S lacks these properties [84]. It is possible that Thau-3 lack of significant anticancer activity goes hand in hand with frenatin 2.3S situation. As CD studies show, Thau-3 acquires an irregular secondary structure (α-helix, random coil and possibly β-sheet portions) and has exhibited a moderate propensity for self-aggregation. These structural characteristics might have a hindering effect by affecting Thau-3 capability of exposing its hydrophobic core to Huh-7 cell membrane's phospholipids. It would be interesting to perform more CD conformational studies with a membrane model composition closer to cancer cells (e.g. POPS:POPC) to further assess Thau-3 interaction with Huh-7 cells. Ooc-1 didn't show any anticancer activity which is interesting when we take into account that this was the only peptide of the test group that caused nearly 10% cell death (500 µM) via apoptosis or necrosis of mammalian healthy cells (Appendix 10) proving its cytotoxic capabilities. Again, it might be a case of inactivity due to excessive self-aggregation or the fact that Ooc-1 is neutrally charged and has low affinity towards PS molecules, thus further conformational studies with cancer cell models could be invaluable in understanding the properties of Ooc-1.

PSo2-2, PSo-4 and PSo-7 proved not to be cytotoxic against healthy cells up to 500 µM concentrations, but exhibited anticancer properties against Huh-7 cells at low µM concentrations (Table 6) when compared to other known peptides that exerted anticancer properties on the same cell line, like cecropinXJ [85] (Table 7). In fact, at 42 µM, PSo2-2 produces a stronger anticancer activity on Huh-7 cells than that demonstrated by cecropinXJ [85] or even by PSo-7 or PSo-4 at higher concentrations. Nevertheless, the very low µM concentrations at which peptides PSo-7 and PSo-4 displayed anticancer activity are more comparable with those for peptides BLP-7 and Bombinin H-BO (Table 7), from the secretions of the Oriental fire-bellied toad, *Bombina orientalis* [86].

The described characteristics of AMPs with anticancer properties, and their modes of action, are in all very similar to those already mentioned for antimicrobial activity.

	Antibacterial activity		Antiparasitic activity	Anticancer activity
	E. coli MIC	*S. aureus* MIC	*T. b. brucei*	Huh-7 cells
	µM	**µM**	**µM**	**µM**
Thaulin-1	24.7	198	-	-
CecropinXJ	-	0.4	-	50
BLP-7	6.3	6.3	-	3.87
Bombinin H-BO	639	159.7	-	1.81
SHP-1	-	-	4	-

Table 7. Antibacterial, antiparasitic and anticancer properties of other literature described peptides [33,76,85,86].

Considering our anticancer active peptides, we can argue that even though they are all cationic, with similar net charges, they show different self-aggregation rates, secondary structures and arrangement of hydrophobic residues in their sequences and therefore might have different modes of action specially when comparing PSo2-2 results with PSo-4 and -7. Furthermore, PSo2-2 showed the second highest rate of self-aggregation, amongst the tested peptides, and a certain level of peptide self-aggregation capability has been reported as beneficial towards cationic peptides anticancer activity [87]. This ability would help peptides to associate with each other as to form transmembrane pores or channels that would ultimately cause cell death [87]. It is needless to say that further tests in relation to interactions of these peptides with cancer membrane models, peptide spatial orientation in relation to the membranes and conformation would be invaluable in further assessing this matter.

As future work moving forward, further optimisation of the XTT and alamarBlue assays for Huh-7 cells and trypanosomes might be necessary as well as further replicates of the peptides' activity against these two targets. Also, it would be important to carry out apoptosis/necrosis assays since these could shed some light as to the mode of action being used by the peptides that showed anticancer activity – PSo-4, PSo-7 and PSo2-2. FTIR analysis alongside further CD studies with POPG:POPC LUVs would allow us to confirm our initial results and to further assess our peptides secondary structure behaviour against other membrane models that mimic Gram-positive bacteria, cancer cells and trypanosomes. It would also be interesting to perform AFM or scanning electron microscopy on affected Huh-7 cells and BSFs of *T. b. brucei* to visually evaluate the sort of damage being induced to the cell membranes.

Another sticking point for this test group would be to investigate self-aggregation occurrence in other solutions or solvents and examine if a decrease or increase in self-

aggregation has any effect on the activity exerted by the peptides. Eventually, nuclear magnetic resonance spectroscopy would be an invaluable tool to study the dynamics of the peptides, their interactions, target recognition and ligand binding events.

This project has allowed us to uncover some of the properties these peptides express in a "crude" state, given that no initial care was taken as to peptide stability in solution before performing the activity assays. As mentioned previously, all of our peptides showed different levels of self-aggregation, which might impair their activity or have the complete opposite effect and enhance their properties. The bottom line is, even though these peptides were tested in an "unrefined" manner, they still displayed a range of activities and that is really encouraging when looking into future research and development that can be applied here.

5 References

1. Hwang AY, Gums JG. The emergence and evolution of antimicrobial resistance: Impact on a global scale. Bioorg Med Chem 2016;24(24):6440–5. doi: 10.1016/j.bmc.2016.04.027

2. Morehead MS, Scarbrough C. Emergence of Global Antibiotic Resistance. Prim Care 2018;45(3):467–84. doi: 10.1016/j.pop.2018.05.006

3. Tacconelli E, Carrara E, Savoldi A, Harbarth S, Mendelson M, Monnet DL, et al. Discovery, research, and development of new antibiotics: the WHO priority list of antibiotic-resistant bacteria and tuberculosis. Lancet Infect Dis 2018;18(3):318–27. doi: 10.1016/S1473-3099(17)30753-3

4. Hwang AY, Gums JG. The emergence and evolution of antimicrobial resistance: Impact on a global scale. Bioorg Med Chem 2016;24(24):6440–5. Table 1, Timeline of antibiotic introduction and identified resistance; p. 6441. doi: 10.1016/j.bmc.2016.04.027

5. Mulani MS, Kamble EE, Kumkar SN, Tawre MS, Pardesi KR. Emerging Strategies to Combat ESKAPE Pathogens in the Era of Antimicrobial Resistance: A Review. Front Microbiol 2019;10. doi: 10.3389/fmicb.2019.00539

6. Cancer treatment and antimicrobial resistance. Lancet Oncol 2013;14(4):265 [Editorial]. doi: 10.1016/S1470-2045(13)70145-1

7. Arruebo M, Vilaboa N, Sáez-Gutierrez B, Lambea J, Tres A, Valladares M, et al. Assessment of the Evolution of Cancer Treatment Therapies. Cancers (Basel) 2011;3(3):3279–330. doi: 10.3390/cancers3033279

8. Felício MR, Silva ON, Gonçalves S, Santos NC, Franco OL. Peptides with Dual Antimicrobial and Anticancer Activities. Front Chem 2017;5(February):1–9. doi: 10.3389/fchem.2017.00005

9. Luqmani YA. Mechanisms of Drug Resistance in Cancer Chemotherapy. Med Princ Pract 2005;14(1):35–48. doi: 10.1159/000086183

10. Nikolaou M, Pavlopoulou A, Georgakilas AG, Kyrodimos E. The challenge of drug resistance in cancer treatment: a current overview. Clin Exp Metastasis 2018;35(4):309–18. doi: 10.1007/s10585-018-9903-0

11. Lohitesh K, Chowdhury R, Mukherjee S. Resistance a major hindrance to chemotherapy in hepatocellular carcinoma: an insight. Cancer Cell Int 2018;18(1):44. doi: 10.1186/s12935-018-0538-7

12. Mitra AK, Mawson AR. Neglected Tropical Diseases: Epidemiology and Global Burden. Trop Med Infect Dis 2017;2(3):36. doi: 10.3390/tropicalmed2030036

13. Uniting to Combat NTDs [Internet]. 2017 [cited 2019 Jan 20]. [Figure], Burden of neglected tropical diseases. Available from: https://unitingtocombatntds.org/wp-content/uploads/2017/11/burden_of_neglected_tropical_diseases.pdf

14. Neglected tropical diseases [Internet]. World Health Organization [cited 2019 Jan 20];Available from: https://www.who.int/neglected_diseases/diseases/en/

15. Molyneux DH. The "Neglected Tropical Diseases": now a brand identity; responsibilities, context and promise. Parasit Vectors 2012;5(1):23.
doi: 10.1186/1756-3305-5-23

16. Rosenberg M, Utzinger J, Addiss DG. Preventive Chemotherapy Versus Innovative and Intensified Disease Management in Neglected Tropical Diseases: A Distinction Whose Shelf Life Has Expired. PLoS Negl Trop Dis 2016;10(4):e0004521.
doi: 10.1371/journal.pntd.0004521

17. Sleeping Sickness - Biology [Internet]. Centers for Disease Control and Prevention 2019 [cited 2019 Feb 3];Available from:
https://www.cdc.gov/parasites/sleepingsickness/biology.html

18. The parasite [Internet]. World Health Organization 2016 [cited 2019 Feb 3];Available from: https://www.who.int/trypanosomiasis_african/parasite/en/

19. Sleeping Sickness Biology [Internet]. Centers for Disease Control and Prevention 2019 [cited 2019 Feb 3]. [Figure], Life Cycle. Available from:
https://www.cdc.gov/parasites/sleepingsickness/biology.html

20. Kennedy PGE, Rodgers J. Clinical and Neuropathogenetic Aspects of Human African Trypanosomiasis. Front Immunol 2019;10(JAN):1–11.
doi: 10.3389/fimmu.2019.00039

21. Kennedy PGE. The continuing problem of human African trypanosomiasis (sleeping sickness). Ann Neurol 2008;64(2):116–26. doi: 10.1002/ana.21429

22. Kennedy PG. Clinical features, diagnosis, and treatment of human African trypanosomiasis (sleeping sickness). Lancet Neurol 2013;12(2):186–94.
doi: 10.1016/S1474-4422(12)70296-X

23. Kennedy PG. Clinical features, diagnosis, and treatment of human African trypanosomiasis (sleeping sickness). Lancet Neurol 2013;12(2):186–94. Table: Drugs used in treatment of human African trypanosomiasis; p. 191.
doi: 10.1016/S1474-4422(12)70296-X

24. Lewies A, Wentzel J, Jacobs G, Du Plessis L. The Potential Use of Natural and Structural Analogues of Antimicrobial Peptides in the Fight against Neglected Tropical Diseases. Molecules 2015;20(8):15392–433.
doi: 10.3390/molecules200815392

25. Haney EF, Straus SK, Hancock REW. Reassessing the Host Defense Peptide Landscape. Front Chem 2019;7(February):1–22. doi: 10.3389/fchem.2019.00043

26. Hancock REW, Sahl H-G. Antimicrobial and host-defense peptides as new anti-infective therapeutic strategies. Nat Biotechnol 2006;24(12):1551–7. doi: 10.1038/nbt1267

27. Ladram A. Antimicrobial peptides from frog skin biodiversity and therapeutic promises. Front Biosci 2016;21(7):4461. doi: 10.2741/4461

28. Bevers E, Comfurius P, Zwaal R. Regulatory Mechanisms in Maintenance and Modulation of Transmembrane Lipid Asymmetry: Pathophysiological Implications. Lupus 1996;5(5):480–7. doi: 10.1177/096120339600500531

29. Kumar P, Kizhakkedathu J, Straus S. Antimicrobial Peptides: Diversity, Mechanism of Action and Strategies to Improve the Activity and Biocompatibility *In Vivo*. Biomolecules 2018;8(1):4. doi: 10.3390/biom8010004

30. Kumar P, Kizhakkedathu J, Straus S. Antimicrobial Peptides: Diversity, Mechanism of Action and Strategies to Improve the Activity and Biocompatibility *In Vivo*. Biomolecules 2018;8(1):4. doi: 10.3390/biom8010004

31. Jenssen H, Hamill P, Hancock RE. Peptide Antimicrobial Agents. Clin Microbiol Rev 2006;19(3):491–511. doi: 10.1128/CMR.00056-05

32. Wang Z. The Antimicrobial Peptide Database [Internet]. [cited 2018 Dec 6];Available from: http://aps.unmc.edu/AP/main.php

33. Marani MM, Perez LO, de Araujo AR, Plácido A, Sousa CF, Quelemes PV, et al. Thaulin-1: The first antimicrobial peptide isolated from the skin of a Patagonian frog *Pleurodema thaul* (Anura: Leptodactylidae: Leiuperinae) with activity against *Escherichia coli*. Gene 2017;605(March):70–80. doi: 10.1016/j.gene.2016.12.020

34. Lata S, Mishra NK, Raghava GP. AntiBP2: improved version of antibacterial peptide prediction. BMC Bioinformatics 2010;11(Suppl 1):S19. doi: 10.1186/1471-2105-11-S1-S19

35. Andrews JM. Determination of minimum inhibitory concentrations. J Antimicrob Chemother 2001;48(suppl_1):5–16. doi: 10.1093/jac/48.suppl_1.5

36. Carvalho FA, Santos NC. Atomic force microscopy-based force spectroscopy - biological and biomedical applications. IUBMB Life 2012;64(6):465–72. doi: 10.1002/iub.1037

37. Atomic Force Microscopy - What is it? [Internet]. Keysight Technologies [cited 2019 Aug 6];Available from: https://www.keysight.com/main/editorial.jspx?ckey=1774141&lc=eng&cc=PT

38. Atomic Force Microscopy - What is it? [Internet]. Keysight Technologies [cited 2019 Aug 6]. [Figure], AFM Schematic. Available from: https://www.keysight.com/main/editorial.jspx?ckey=1774141&lc=eng&cc=PT

39. Cell Proliferation Kit II (XTT) - Colorimetric assay (XTT based) for the non-radioactive quantification of cell proliferation and viability [Internet]. Roche 2016 [cited 2019 Mar 15];Available from: https://www.sigmaaldrich.com/content/dam/sigma-aldrich/docs/Roche/Bulletin/1/11465015001bul.pdf

40. Roehm NW, Rodgers GH, Hatfield SM, Glasebrook AL. An improved colorimetric assay for cell proliferation and viability utilizing the tetrazolium salt XTT. J Immunol Methods 1991;142(2):257–65. doi: 10.1016/0022-1759(91)90114-u

41. XTT Cell Proliferation Assay Kit [Internet]. American Type Culture Collection 2011 [cited 2019 Mar 5];1–6. Figure 2, The Colorimetric Reduction of XTT by Cellular Enzymes; p. 1. Available from: https://www.atcc.org/~/media/56374CEEC36C47159D2040410828B969.ashx

42. Rampersad SN. Multiple Applications of Alamar Blue as an Indicator of Metabolic Function and Cellular Health in Cell Viability Bioassays. Sensors (Basel) 2012;12(9):12347–60. doi: 10.3390/s120912347

43. Wang W, Singh SK, Li N, Toler MR, King KR, Nema S. Immunogenicity of protein aggregates - Concerns and realities. Int J Pharm 2012;431(1–2):1–11. doi: 10.1016/j.ijpharm.2012.04.040

44. DeWitte RS. Avoiding physicochemical artefacts in early ADME – Tox experiments. Drug Discov Today 2006;11(17–18):855–9. doi: 10.1016/j.drudis.2006.07.012

45. Moussa EM, Panchal JP, Moorthy BS, Blum JS, Joubert MK, Narhi LO, et al. Immunogenicity of Therapeutic Protein Aggregates. J Pharm Sci 2016;105(2):417–30. doi: 10.1016/j.xphs.2015.11.002

46. Henriques ST, Pattenden LK, Aguilar M-I, Castanho MARB. PrP(106-126) Does Not Interact with Membranes under Physiological Conditions. Biophys J 2008;95(4):1877–89. doi: 10.1529/biophysj.108.131458

47. Figueira TN, Palermo LM, Veiga AS, Huey D, Alabi CA, Santos NC, et al. *In Vivo* Efficacy of Measles Virus Fusion Protein-Derived Peptides Is Modulated by the Properties of Self-Assembly and Membrane Residence. J Virol 2017;91(1):1–17. doi: 10.1128/JVI.01554-16

48. Greenfield NJ. Using circular dichroism spectra to estimate protein secondary structure. Nat Protoc 2006;1(6):2876–90. doi: 10.1038/nprot.2006.202

49. Kelly SM, Jess TJ, Price NC. How to study proteins by circular dichroism. Biochim Biophys Acta Proteins Proteom 2005;1751(2):119–39. doi: 10.1016/j.bbapap.2005.06.005

50. Hurlburt N. Circular Dichroism [Internet]. LibreTexts2019 [cited 2019 Aug 9];Available from: https://chem.libretexts.org/Bookshelves/Physical_and_Theoretical_Chemistry_Text book_Maps/Supplemental_Modules_(Physical_and_Theoretical_Chemistry)/Spectr oscopy/Electronic_Spectroscopy/Circular_Dichroism#title

51. Circular dichroism [Internet]. Wikipedia 2019 [cited 2019 Aug 9]. [Figure], Linearly and Circularly polarized. Available from: https://en.wikipedia.org/wiki/Circular_dichroism

52. Hurlburt N. Circular Dichroism [Internet]. LibreTexts2019 [cited 2019 Aug 9]. [Figure 4], Elliptically polarized light. Available from: https://chem.libretexts.org/Bookshelves/Physical_and_Theoretical_Chemistry_Text book_Maps/Supplemental_Modules_(Physical_and_Theoretical_Chemistry)/Spectr oscopy/Electronic_Spectroscopy/Circular_Dichroism#title

53. Bobbitt DR. Chapter 2 Instrumentation for the measurement of circular dichroism; past, present and future developments. In: Purdie N, Brittain HG, editors. Analytical Applications of Circular Dichroism. Amsterdam: Elsevier B.V.; 1994. page 15–52. doi: 10.1016/S0167-9244(08)70175-6

54. Hurlburt N. Circular Dichroism [Internet]. LibreTexts2019 [cited 2019 Aug 9]. [Figure 5], The instrumentation for a common CD spectrometer. Available from: https://chem.libretexts.org/Bookshelves/Physical_and_Theoretical_Chemistry_Text book_Maps/Supplemental_Modules_(Physical_and_Theoretical_Chemistry)/Spectr oscopy/Electronic_Spectroscopy/Circular_Dichroism#title

55. Santos NC, Castanho MARB. An overview of the biophysical applications of atomic force microscopy. Biophys Chem 2004;107(2):133–49. doi: 10.1016/j.bpc.2003.09.001

56. Towell JF, Manning MC. Chapter 6 Analysis of protein structure by circular dichroism spectroscopy. In: Purdie N, Brittain HG, editors. Techniques and Instrumentation in Analytical Chemistry. Amsterdam: Elsevier B.V.; 1994. page 175–205.doi: 10.1016/S0167-9244(08)70179-3

57. Greenfield NJ. Analysis of the kinetics of folding of proteins and peptides using circular dichroism. Nat Protoc [Internet]. 2006 [cited 2019 Aug 9];1(6):2891–9. Figure 1b, CD spectra of representative proteins with varying conformations; p. 21. Available from: https://www.researchgate.net/publication/6414497_Greenfield_NJ_Using_circular_ dichroism_spectra_to_estimate_protein_secondary_structure_Nat_Protoc_1_2876-2890/figures

58. *Escherichia coli* (Migula) Castellani and Chalmers (ATCC® 25922™) [Internet]. American Type Culture Collection 2016 [cited 2019 Feb 9];Available from: https://www.lgcstandards-atcc.org/products/all/BAA-1427.aspx?geo_country=be

59. *Staphylococcus aureus* subsp. *aureus* Rosenbach (ATCC® 25923™) [Internet]. American Type Culture Collection 2016 [cited 2019 Feb 9];Available from: https://www.lgcstandards-atcc.org/Products/All/25923.aspx?geo_country=pt

60. CLSI. Methods for Dilution Antimicrobial Susceptibility Tests for Bacteria That Grow Aerobically ; Approved Standard — Ninth Edition. CLSI document M07-A9. Wayne, PA: Clinical and Laboratory Standards Institute; 2012.

61. Minimum Inhibitory Concentration (MIC) and Minimum Bactericidal Concentration (MBC) Assay [Internet]. Emery Pharma 2019 [cited 2019 Feb 10]. [Figure], MIC and MBC Assays. Available from: https://emerypharma.com/biology/minimum-inhibitory-concentration/

62. EUCAST. Breakpoint tables for interpretation of MICs and zone diameters. Version 9.0. The European Committee on Antimicrobial Susceptibility Testing; 2019.

63. Peacock L, Ferris V, Bailey M, Gibson W. Fly transmission and mating of *Trypanosoma brucei brucei* strain 427. Mol Biochem Parasitol 2008;160(2):100–6. doi: 10.1016/j.molbiopara.2008.04.009

64. Cross GAM, Manning JC. Cultivation of *Trypanosoma brucei* sspp. in semi-defined and defined media. Parasitology 1973;67(3):315–31. doi: 10.1017/s0031182000046540

65. Lister 427 Lineage [Internet]. The Rockefeller University [cited 2019 Jul 27];Available from: http://tryps.rockefeller.edu/DocumentsGlobal/lineage_Lister427.pdf

66. Hirumi H, Hirumi K. Continuous Cultivation of *Trypanosoma brucei* Blood Stream Forms in a Medium Containing a Low Concentration of Serum Protein without Feeder Cell Layers. J Parasitol 1989;75(6):985.

67. Krelle AC, Okoli AS, Mendz GL. Huh-7 Human Liver Cancer Cells: A Model System to Understand Hepatocellular Carcinoma and Therapy. J Cancer Ther 2013;04(02):606–31. doi: 10.4236/jct.2013.42078

68. Nakabayashi H, Taketa K, Miyano K, Yamane T, Sato J. Growth of human hepatoma cells lines with differentiated functions in chemically defined medium. Cancer Res 1982;42(9):3858–63.

69. Faustino AF, Guerra GM, Huber RG, Hollmann A, Domingues MM, Barbosa GM, et al. Understanding Dengue Virus Capsid Protein Disordered N-Terminus and pep14-23-Based Inhibition. ACS Chem Biol 2015;10(2):517–26. doi: 10.1021/cb500640t

70. Pazderková M, Maloň P, Zíma V, Hofbauerová K, Kopecký V, Kočišová E, et al. Interaction of Halictine-Related Antimicrobial Peptides with Membrane Models. Int J Mol Sci 2019;20(3):631. doi: 10.3390/ijms20030631

71. Wallace BA, Janes RW. Synchrotron radiation circular dichroism (SRCD) spectroscopy: an enhanced method for examining protein conformations and protein interactions. Biochem Soc Trans 2010;38(4):861–73. doi: 10.1042/BST0380861

72. Li J, Koh J-J, Liu S, Lakshminarayanan R, Verma CS, Beuerman RW. Membrane Active Antimicrobial Peptides: Translating Mechanistic Insights to Design. Front Neurosci 2017;11. doi: 10.3389/fnins.2017.00073

73. Malanovic N, Lohner K. Gram-positive bacterial cell envelopes: The impact on the activity of antimicrobial peptides. Biochim Biophys Acta Biomembr 2016;1858(5):936–46. doi: 10.1016/j.bbamem.2015.11.004

74. Scott MG, Gold MR, Hancock RE. Interaction of cationic peptides with lipoteichoic acid and gram-positive bacteria. Infect Immun 1999;67(12):6445–53. PMID: 10569762

75. Smith TK, Bütikofer P. Lipid metabolism in *Trypanosoma brucei*. Mol Biochem Parasitol 2010;172(2):66–79. doi: 10.1016/j.molbiopara.2010.04.001

76. Harrington JM, Widener J, Stephens N, Johnson T, Francia M, Capewell P, et al. The Plasma Membrane of Bloodstream-form African Trypanosomes Confers Susceptibility and Specificity to Killing by Hydrophobic Peptides. J Biol Chem 2010;285(37):28659–66. doi: 10.1074/jbc.M110.151886

77. Shimogawa MM, Saada EA, Vashisht AA, Barshop WD, Wohlschlegel JA, Hill KL. Cell Surface Proteomics Provides Insight into Stage-Specific Remodeling of the Host-Parasite Interface in *Trypanosoma brucei*. Mol Cell Proteomics 2015;14(7):1977–88. doi: 10.1074/mcp.M114.045146

78. Schweizer F. Cationic amphiphilic peptides with cancer-selective toxicity. Eur J Pharmacol 2009;625(1–3):190–4. doi: 10.1016/j.ejphar.2009.08.043

79. Dathe M, Nikolenko H, Meyer J, Beyermann M, Bienert M. Optimization of the antimicrobial activity of magainin peptides by modification of charge. FEBS Lett 2001;501(2–3):146–50. doi: 10.1016/s0014-5793(01)02648-5

80. Sokalingam S, Raghunathan G, Soundrarajan N, Lee S-G. A Study on the Effect of Surface Lysine to Arginine Mutagenesis on Protein Stability and Structure Using Green Fluorescent Protein. PLoS One 2012;7(7):e40410. doi: 10.1371/journal.pone.0040410

81. Vaara M. Agents that increase the permeability of the outer membrane. Microbiol Rev 1992;56(3):395–411. PMID: 1406489

82. Martínez-García M, Bart J-M, Campos-Salinas J, Valdivia E, Martínez-Bueno M, González-Rey E, et al. Autophagic-related cell death of *Trypanosoma brucei* induced by bacteriocin AS-48. Int J Parasitol Drugs Drug Resist 2018;8(2):203–12. doi: 10.1016/j.ijpddr.2018.03.002

83. Harrington JM. Antimicrobial peptide killing of African trypanosomes. Parasite Immunol 2011;33(8):461–9. doi: 10.1111/j.1365-3024.2011.01294.x

84. Conlon JM, Mechkarska M, Radosavljevic G, Attoub S, King JD, Lukic ML, et al. A family of antimicrobial and immunomodulatory peptides related to the frenatins from skin secretions of the Orinoco lime frog *Sphaenorhynchus lacteus* (Hylidae). Peptides 2014;56:132–40. doi: 10.1016/j.peptides.2014.03.020

85. Xia L, Wu Y, Ma J, Yang J, Zhang F. The antibacterial peptide from *Bombyx mori* cecropinXJ induced growth arrest and apoptosis in human hepatocellular carcinoma cells. Oncol Lett 2016;12(1):57–62. doi: 10.3892/ol.2016.4601

86. Zhou C, Wang Z, Peng X, Liu Y, Lin Y, Zhang Z, et al. Discovery of two bombinin peptides with antimicrobial and anticancer activities from the skin secretion of Oriental fire-bellied toad, *Bombina orientalis*. Chem Biol Drug Des 2018;91(1):50–61. doi: 10.1111/cbdd.13055

87. Huang YB, Wang XF, Wang HY, Liu Y, Chen Y. Studies on Mechanism of Action of Anticancer Peptides by Modulation of Hydrophobicity Within a Defined Structural Framework. Mol Cancer Ther 2011;10(3):416–26. doi: 10.1158/1535-7163.MCT-10-0811

6 Appendix

Appendix 1: *Escherichia coli* strain used in this work

Strain	Characteristics	Origin
ATCC® 25922™	Serotype O6, Biotype 1	Laboratory stock

Appendix 2: *Staphylococcus aureus* subsp. *aureus* strain used in this work

Strain	Characteristics	Origin
ATCC® 25923™	-	Laboratory stock

Appendix 3: *Trypanosoma brucei* subsp. *brucei* strains used in this work

Strain	Characteristics	Origin
Lister 427 VSG 221 (bloodstream form)	Wild type bloodstream form Expresses variant surface glycoprotein (VSG) 221	Laboratory stock

Appendix 4: Cell line used in this work

Cell Line	Species of Origin	Tissue of Origin	Morphology	Characteristics	Origin
Huh-7	Human	Liver	Epithelial-like	Well differentiated hepatocellular carcinoma	Laboratory stock

Appendix 5: HMI-11 medium

	Volume	Description	Final concentration
IMDM	429 ml	Gibco, Paisley, UK	-
L-Glutamine	-	4 mM	3.4 mM
HEPES	-	25 mM	21.5 mM
Foetal Bovine Serum (Heat Inactivated)	50 ml	Gibco, Paisley, UK	10%
Hypoxanthine (13.6 mg/ml)	5 ml	Sigma-Aldrich, St. Louis, MO, USA	1 mM
L-Cysteine (18.2 mg/ml)	5 ml	Sigma-Aldrich, St. Louis, MO, USA	1.5 mM
Thymidine (39 mg/ml)	0.5 ml	Sigma-Aldrich, St. Louis, MO, USA	0.16 mM
Pyruvic acid (98%)	34.6 µl	Sigma-Aldrich, St. Louis, MO, USA	1 mM
Bathocuproinedisulfonic acid (28.2 mg/ml)	0.5 ml	Sigma-Aldrich, St. Louis, MO, USA	0.05 mM
2-mercaptoethanol (100mM)	1 ml	Sigma-Aldrich, St. Louis, MO, USA	0.2 mM

Appendix 6: RPMI-1640 modified medium

	Volume	Description	Final concentration
RPMI-1640	220 ml	Gibco, Paisley, UK	-
L-Glutamine	-	2.05 mM	1.8 mM
HEPES	-	25 mM	22 mM
Foetal Bovine Serum (Heat Inactivated)	25 ml	Sigma-Aldrich, St. Louis, MO, USA	10%
(MEM NEAA) Minimum Essential Medium Non-Essential Amino Acids (100X)	2.5 ml	Gibco, Paisley, UK	1%
Pen-Strep 10 000 U Penicillin/ml 10 000 U Streptomycin/ml	2.5 ml	Lonza, Verviers, Belgium	1%

Appendix 7: AFM height (A) and amplitude (B) images of MH media

A   B
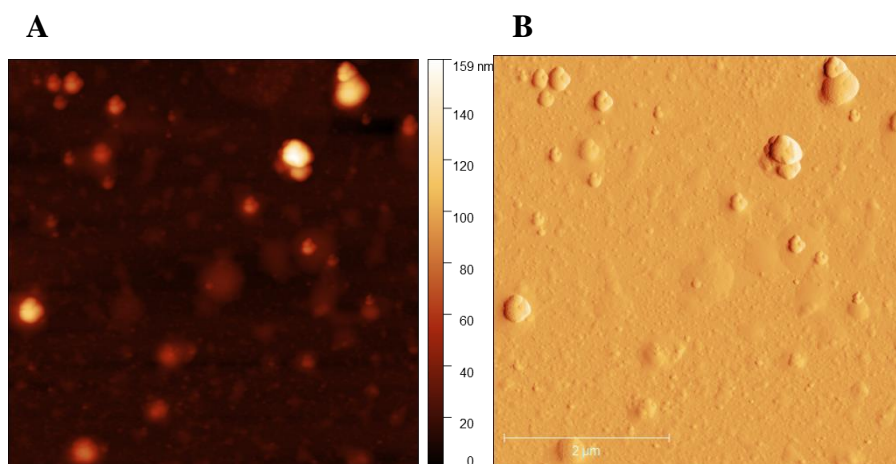
Appendix 8: Optimisation results for *T. b. brucei* (BSF) alamarBlue assay
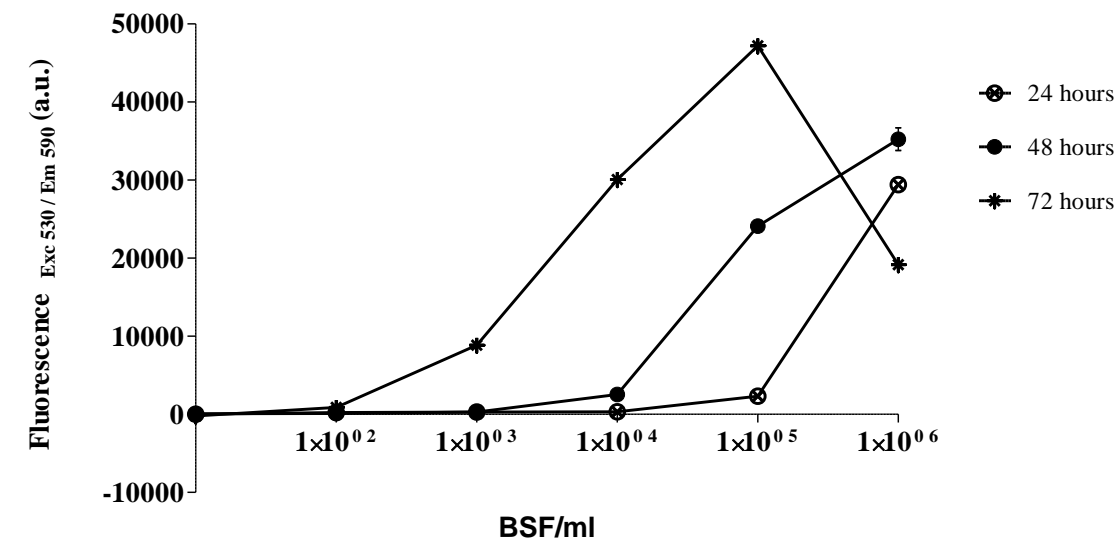
Error bars signify mean (SD).

Appendix 9: Optimisation results for Huh-7 cells XTT assay
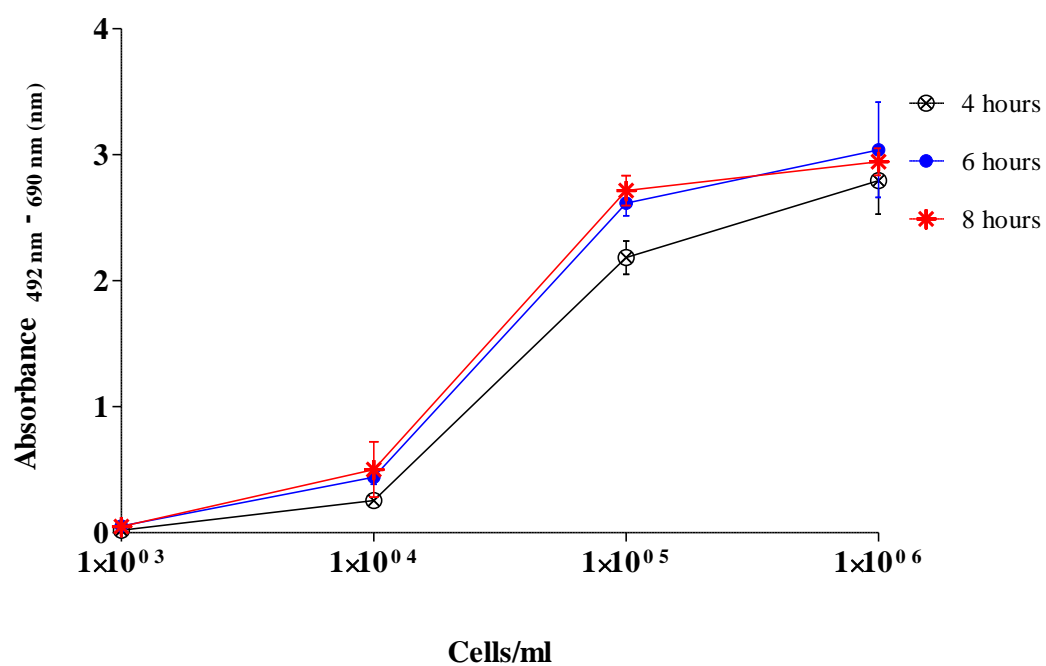

Error bars signify mean (SD).

**Appendix 10:** Evaluation of apoptosis/necrosis capability of our Patagonian amphibian peptides on healthy cells.
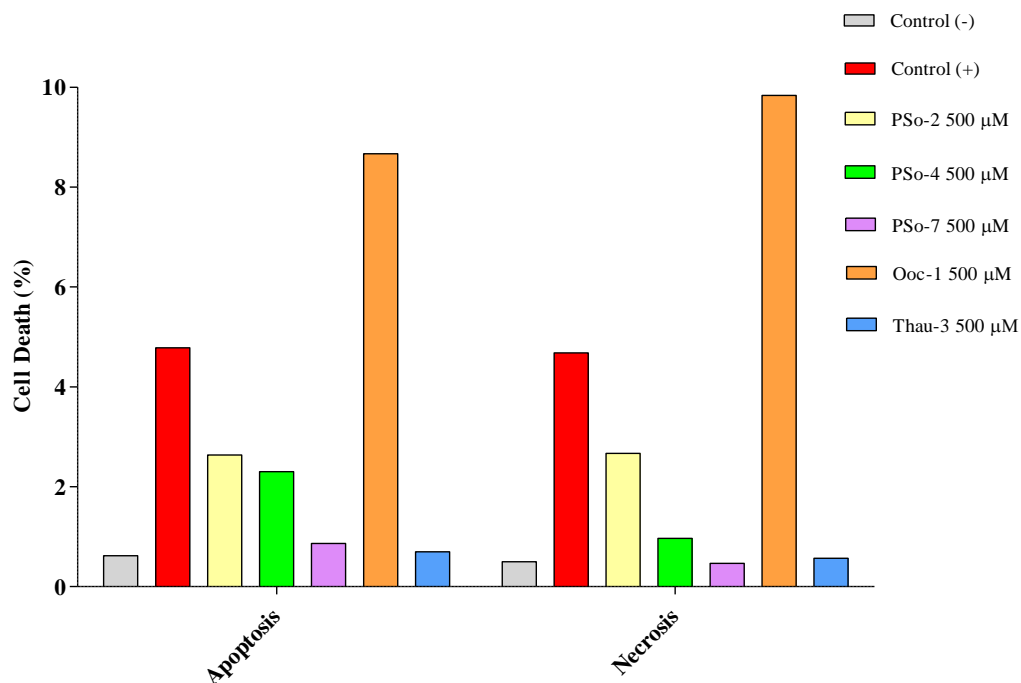

J774.2 cell line from mouse BALB/C (monocyte macrophage) was used as a "healthy" cell line to test for the apoptotic/necrotic capability of our peptides. This assay was performed in Brazil by one of the PhD students from Nuno Santos Lab – iMM, Constança P. Amaral. The experiment was performed once, in triplicate, with an apoptosis/necrosis kit and assessed by flow cytometry.
Control (-) represents untreated cells; Control (+) signifies cells treated with toxic levels of DMSO.

Appendix 11: ANS aggregation assay – PSo-7 spectra replicates
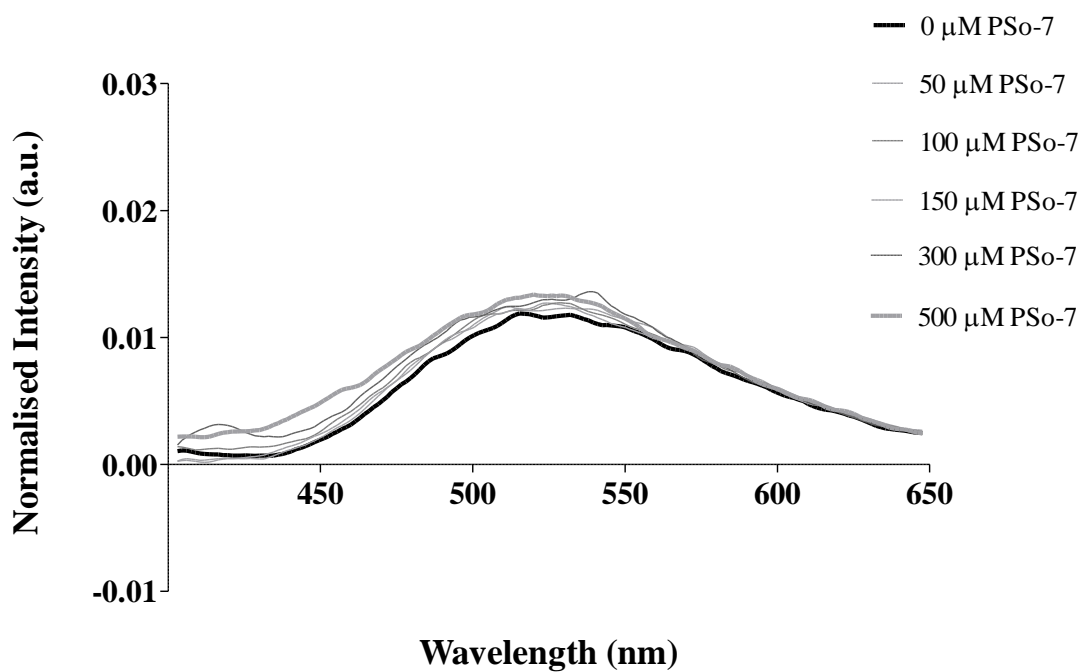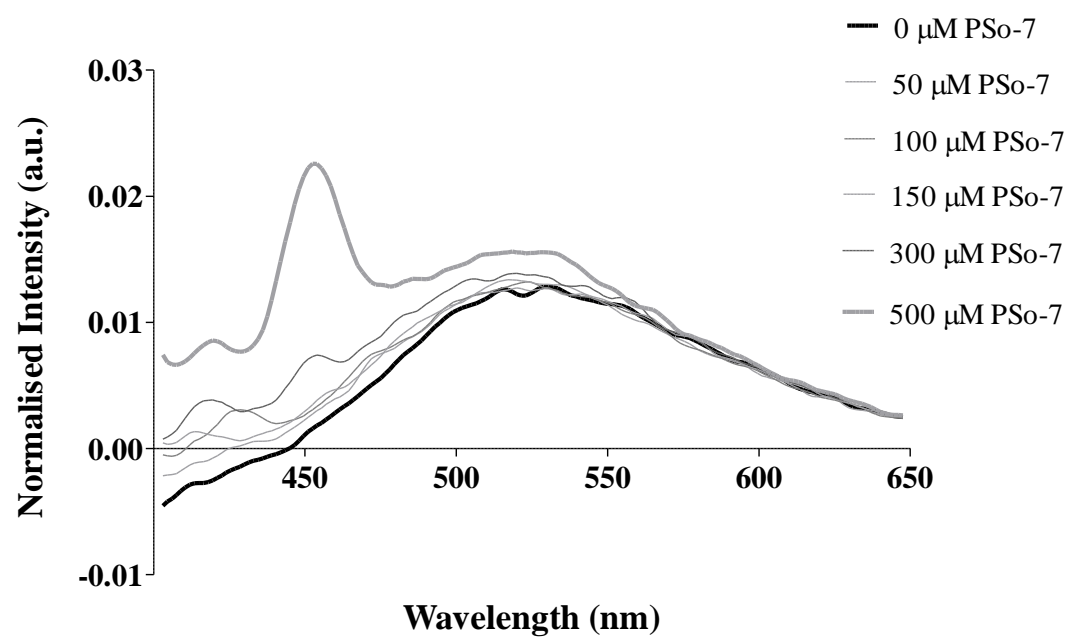
Appendix 12: ANS aggregation assay – PSo-4 spectra replicates
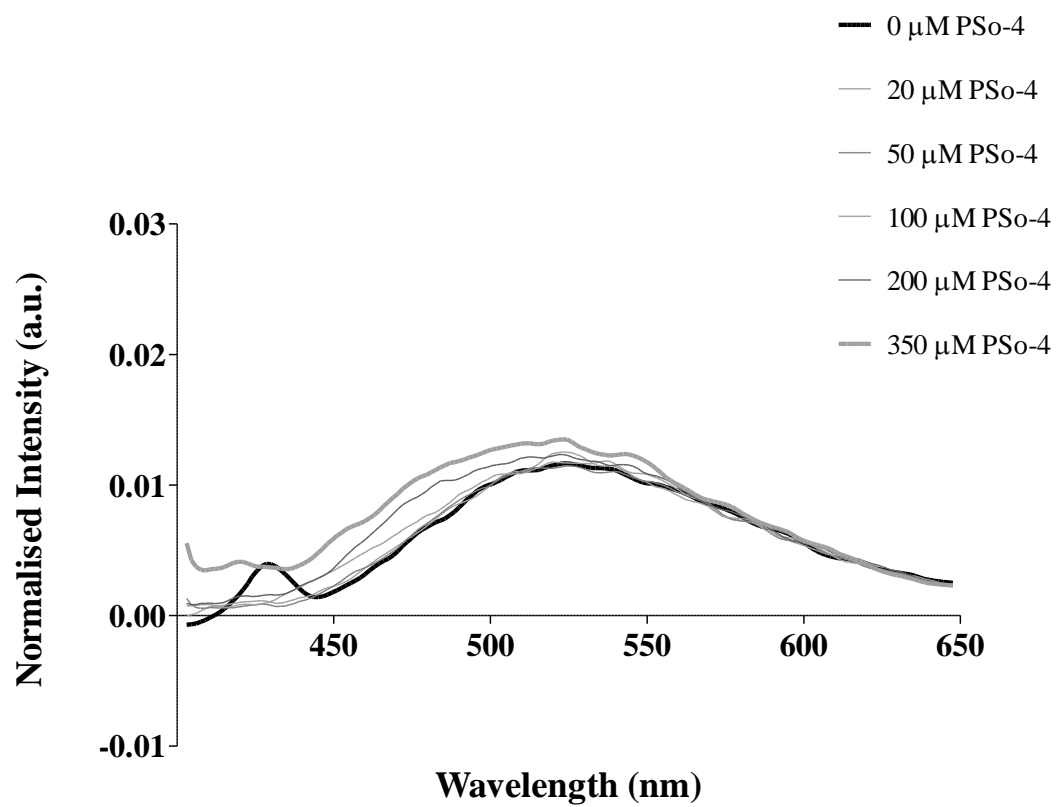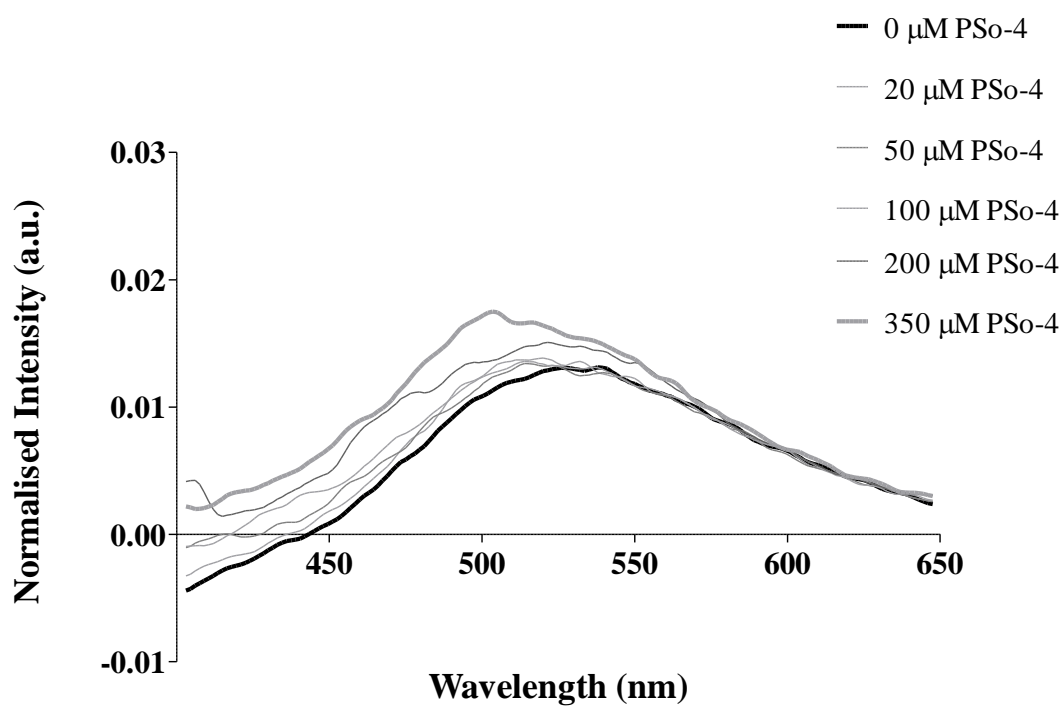
Appendix 13: ANS aggregation assay – Thau-3 spectra replicates
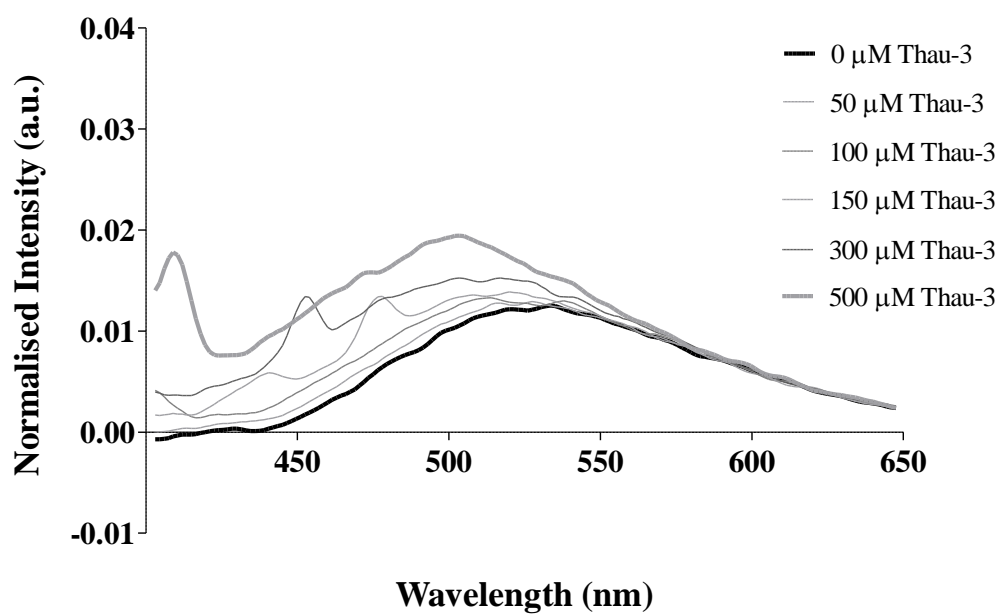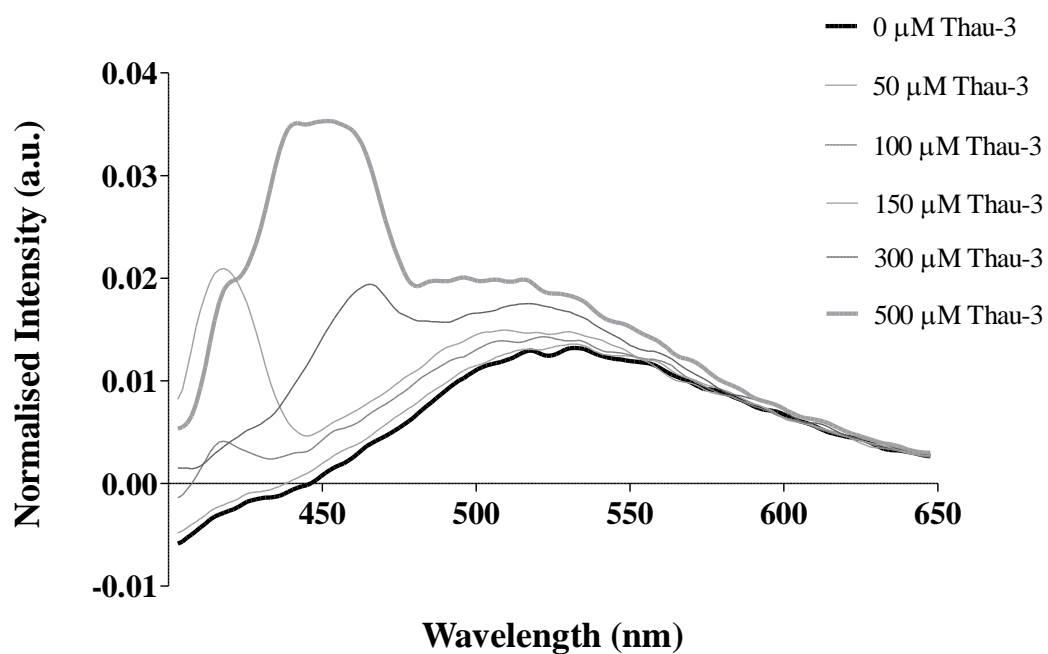
Appendix 14: ANS aggregation assay – PSo2-2 spectra replicates
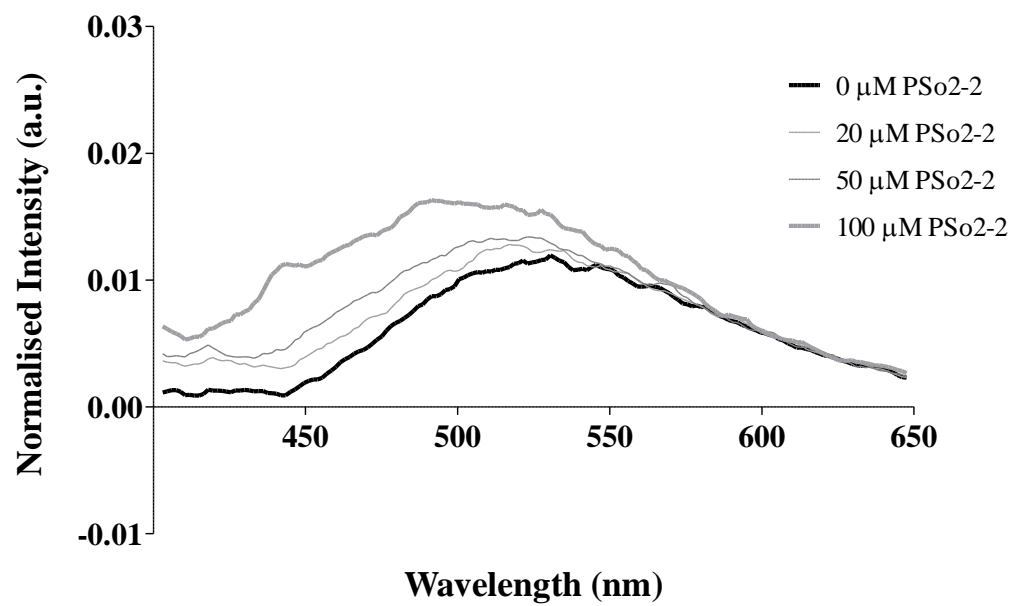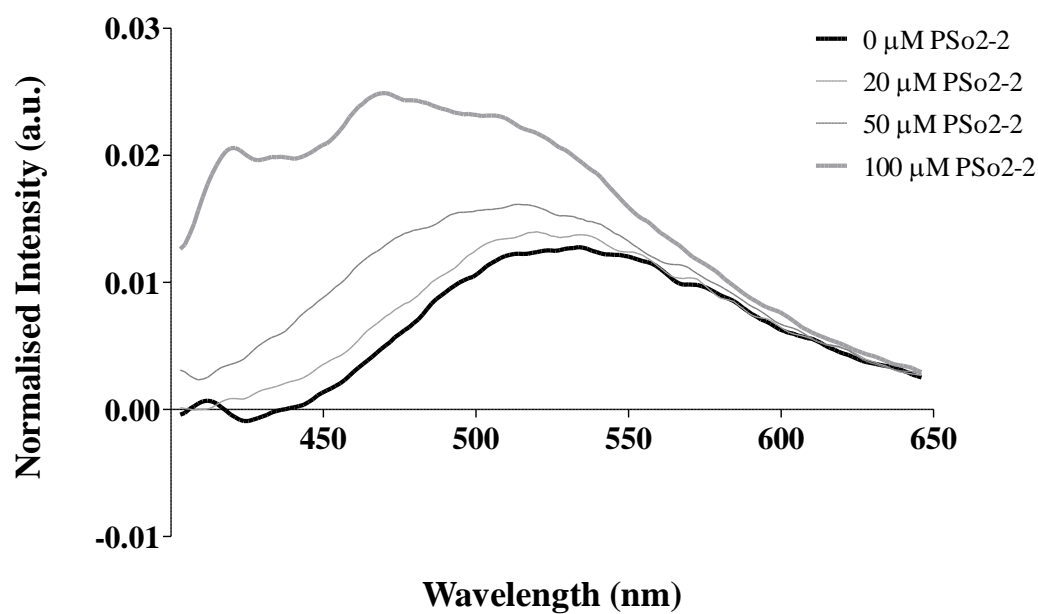
Appendix 15: ANS aggregation assay – Ooc-1 spectra replicates
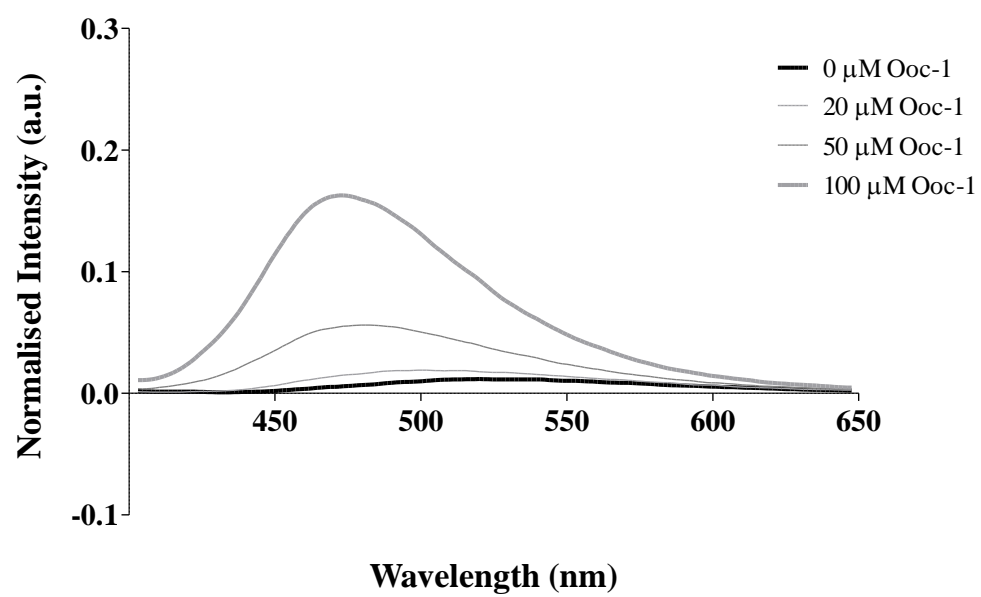
Appendix 16: CD spectrum of PBS with increasing concentrations of POPC:POPG